Durability of a recombination catalyst-based membrane-electrode assembly for electrolysis operation at high current density

Fabiola Pantò, Stefania Siracusano, Nicola Briguglio, Antonino Salvatore Aricò*

CNR-ITAE Institute of Advanced Energy Technologies, National Research Council

Via Salita S. Lucia sopra Contesse 5, 98126 Messina, Italy

**Corresponding author: Tel.: +39 090 624237; fax: +39 090 624247. E-mail address: arico@itae.cnr.it*

Abstract

Hydrogen production through polymer electrolyte membrane water electrolysis was investigated at high current density (4 A cm^{-2}). A PtCo recombination catalyst-based membrane-electrode assembly (MEA) was assessed in terms of performance, efficiency and durability. The electrolysis cell consisted of a thin (50 µm) perfluorosulfonic acid membrane and low platinum group metals (PGM) catalyst loadings (0.6 mg_{MEA} PGM cm^{-2}). An unsupported PtCo catalyst was successfully integrated in the anode. A composite catalytic layer made of IrRuOx and PtCo assisted both oxygen evolution and oxidation of hydrogen permeated through the membrane. The cell voltage for the recombination catalyst-based MEA was about 30 mV lower than the bare MEA during a 3500 h durability test. The modified MEA showed low performance losses during 3500 hours operation at high current density (4 A cm^{-2}) with low catalyst loadings. A decay rate of 9 µV/h was observed in the last 1000 hours. These results are promising for decreasing the capital costs of polymer electrolyte membrane electrolysers. Moreover, the stable voltage efficiency of about 80% vs. the high heating value (HHV) of hydrogen at 4 A cm^{-2}, here achieved, appears very promising to decrease operating expenditures.

Keywords: PtCo Recombination catalyst; Polymer electrolyte membrane electrolysis; Hydrogen; Low catalyst loadings; High current density operation, Steady-state durability tests.

1. Introduction

The transition from fossil fuels to renewable energy sources (RES) requires developing efficient and high energy density energy storage systems [1–8]. Water electrolysers represent nowadays a suitable technology to better integrate renewables and to comply with their discontinuity by providing grid-balancing service [9–14]. The excess of renewable energy that is now curtailed by the grid operators when the demand is low may be efficiently converted to hydrogen [1-14]. This can be used directly as fuel for sustainable mobility applications or stored and converted again into electrical energy when needed [1–9,11,15–18].

Electrochemical water splitting technologies, based on RES, appear today as the most promising processes to produce “green hydrogen” in an economically and environmentally sustainable way [1,9,11,13,17–19]. Among the various water electrolysis technologies, polymer electrolyte membrane (PEM) electrolysis systems show high operating current densities, good efficiency and proper dynamic behaviour. These systems are characterised by rapid response, fast start-up and suitable characteristics for interfacing with RES and electricity grid [4,8,14,17,19–24].

With respect to other electrolysis devices, PEM systems are able to produce green and high-pressure hydrogen with excellent gas purity while working under high differential pressures [4,12,14,19,25,26]. The capability of these systems to generate pressurised hydrogen appears very convenient since they can reduce the need of a further expensive

and less efficient process for mechanical gas compression, at least in applications dealing with hydrogen injection into the gas grid (power-to-gas) [3,4,8,13,16,17,19]. For refuelling stations application, high pressure PEM electrolysers can minimise the energy losses in the post-compression process [19,27].

However, some issues need to be overcome for a large-scale deployment of this technology. Safety issues, related to the operation at high differential pressures, and cost of electrolysis systems are among the main drawbacks [4,18,19,23,25,28–32].

The capability of the PEM system to work under asymmetric pressure conditions (by pressurising only the cathode compartment) reduces the corrosion of the metallic components at the anode and the hazards of fire and explosion due to the presence of pressurised oxygen [33]. On the other hand, hydrogen permeation towards the anode compartment, may cause, especially at low partial loads (below 20%), the risk of flammability occurrence [27,31,34–37]. At low current density, the hydrogen concentration in the oxygen stream is usually high and a shutdown of electrolyser is required for safety reasons when this concentration reaches 2-3 % vol. Different strategies have been developed to improve the electrolysers safety characteristics and to provide an oxidation and/or recombination route for the hydrogen permeated to the anode. Among the different routes that involve catalyst and membrane modifications [21, 38–42], an innovative approach was based on the use of a hydrogen oxidation catalyst at the interface with a perfluorosulfonic (PFSA) membrane and an anode catalyst layer [36]. The advantage of this strategy lies in the possibility of increasing the operating pressure of electrolyser without endangering safety characteristics and operating load range. Another approach deals with the formation of a membrane interlayer based on Pt recombination particles for reducing the anodic hydrogen content in PEM water electrolysis [21,41].

Beside the safety aspects, relevant efforts have been also addressed to reduce the costs of electrolysers by focusing on system operation at higher current density and on the use of lower amounts of precious metals [34,36,43–45]. PEM electrolysers can effectively operate at high current density (4 A·cm^{-2}) while keeping cutting-edge efficiency [34]. This allows maximising the hydrogen production rate thus reducing capital costs. At high current density, ohmic losses are prevailing in the polarisation curves causing relevant efficiency decrease [3,6]. Ohmic losses can be reduced by using thinner membranes to achieve a voltage efficiency gain [26,34,36,44]. Benchmark membranes for PEM electrolysis are usually thicker than 100 µm (e.g. Nafion® 112 and 117 membranes are 120 and 170 µm thick, respectively). Thus, the performance of a PEM electrolysis cell would benefit from using a membrane much thinner than 100 µm especially at high current density. Nevertheless, the increase of hydrogen crossover rate is inversely related to the thickness of the membrane. Thus, a thin membrane approach requires using specific mitigation strategies such as a recombination or oxidation catalyst integrated into the anode or the membrane. Thus, the two aspects of achieving high current density at proper voltage efficiency by using thin membranes and keeping low the hydrogen concentration in the oxygen stream are strongly interrelated.

The harsh environment of PEM electrolysis, determined by a combination of strong acidic conditions and high operating electrochemical potentials at the anode, imposes the use of precious elements from the platinum group metals (PGM). These are needed for both oxygen evolution and recombination catalysts [46-47] especially if the recombination or oxidation catalysts for permeated hydrogen are integrated into the anode catalyst layer of the membrane-electrode assembly. Both oxygen evolution catalysts (usually based on an Ir-oxide [43,48–52]) and recombination catalysts (often consisting of Pt or Pt-alloys

[21,26,36,40–41]) need to be minimised in term of loadings to reduce their impact on the system cost.

This work deals with enhanced water electrolysis for producing low carbon hydrogen to contribute in decarbonising the next generation energy system. The work addresses the relevant aspects of cell operation at high current density (4 A cm^{-2}) in the presence of low catalyst loadings with the aim of decreasing the capital costs and enhancing the safety characteristics of water electrolysers.

In particular, the objective of the present study is to assess the durability characteristics of a PEM electrolysis membrane-electrode-assembly (MEA) based on a thin membrane and a recombination catalyst integrated into the anode. The latter provides a mitigation strategy for reducing the hydrogen concentration in the oxygen stream. The aim is also to demonstrate that this approach can allow achieving high efficiency characteristics during operation at high current density as required to minimize both capital costs and operating expenditures for the PEM electrolysis system. In particular, to make these systems economically competitive, there is the need to keep the electrolyser under operation even when the cost of renewable energy is relatively high. In this regard, the system efficiency plays an important role.

In this work, IrRuOx and Pt/C electrocatalysts have been used as anode and cathode catalysts, respectively. Low PGM loadings of 0.3 mg_{Ir+Ru} cm^{-2} for the IrRuOx catalyst at the anode and 0.1 mg Pt cm^{-2} at the cathode were used in the bare MEA. A thin perfluorosulfonic acid (PFSA) membrane of 50 µm thickness was used to reduce the ohmic losses at high current density.

In a previous work from our group [36], a PtCo alloy was deposited onto a PFSA membrane to act as hydrogen oxidation promoter forming an interface with the outer Ir-oxide anode catalyst layer [36]. The PtCo recombination catalyst was also investigated in

a mixed configuration with the oxygen evolution catalyst (IrRuOx) [26]. In both cases, the PtCo catalyst showed the capability to decrease the hydrogen crossover in the presence of relatively thin membranes. The mixed configuration showed enhanced recombination activity but lower electrochemical performance compared to the two separate layers [26]. This approach demonstrated the possibility of extending the partial load operation reducing the safety issues. However, no relevant durability studies have been yet carried out for PtCo-recombination catalyst-integrated MEAs. This study aims at covering this gap.

Accordingly, in the present study, a PtCo recombination catalyst (RC) was synthesised, optimised and integrated within the anode structure of a PEM electrolysis MEA. A composite catalyst layer made of a mixture of IrRuOx and PtCo was used at the anode compartment. The metal loading was 0.2 mg cm^{-2} PtCo and 0.3 mg cm^{-2} Ir + Ru. Membrane-electrode-assemblies with the integrated PtCo catalyst (mixed RC MEA) or without (bare MEA) were compared in terms of performance and durability. Good stability was achieved for both systems in durability tests of about 3500 h at a current density of 4 A cm^{-2}.

2. Experimental

2.1. Synthesis of IrRuOx, PtCo and Pt/C electrocatalysts

An unsupported IrRuOx (70% at. Ir: 30% at. Ru) electrocatalyst was prepared by using a modified Adams fusion method [53]. Iridium (IV) and ruthenium (III) hydrate chlorides were supplied by Strem Chemicals and added as metal precursors to isopropanol. After the solubilisation of these precursors and the addition of a finely ground $NaNO_3$ powder, the mixture was heated at 100 °C in air until the complete evaporation of the solvent. The obtained powder was treated in air at 500 °C for 15 minutes. The oxide was thoroughly

washed with distilled water in order to remove sodium chlorides and purified further by using a pre-leaching treatment in $HClO_4$ 0.1 M at 80 °C for 15 minutes.

A 40 wt.% supported Pt on Ketjenblack® carbon (Pt/C) and an unsupported Pt-Co alloy (85:15 at. %) were synthesized by means of the sulphite-complex route [36,44,46]. Hydrate chloroplatinic acid and cobalt chloride (provided by Merck) were used to prepare the corresponding sulphite precursors [36,54].

For the Pt/C catalyst, Ketjenblack® carbon was dispersed in distilled water through an ultrasonic bath at 80 °C and a proper amount of platinum sulphite was added to the slurry to obtain the carbon-supported Pt/C cathode catalyst. More details about the catalyst preparation procedure are reported elsewhere [44].

In the case of the unsupported PtCo catalyst, the relative sulphite precursors, in appropriate stoichiometric amounts, were decomposed by the use of hydrogen peroxide. A precipitate was obtained by heating the solution at 70° C. This was filtered and then dried in air at room temperature. The formed amorphous oxides were reduced in diluted hydrogen (10% vol. H_2 in helium at 150 °C in order to favour the formation of a crystalline alloy) and the resulting catalysts were pre-leached in 0.5 M perchloric acid at 80° C to remove impurities.

The unsupported catalysts were finally ball milled at 300 rpm for 2 hours to facilitate the spray deposition process during the MEAs manufacturing. No ball milling procedure was required for the Pt/C catalyst.

2.2. Physico-chemical characterisations

The structural and morphological properties of electrode materials were investigated through complementary characterization techniques.

The structural analysis was carried out by X-ray diffraction (XRD) using a Panalytical X-Pert diffractometer equipped with a CuKα as radiation source. The diffraction patterns were interpreted by means of the Joint Committee on Powder Diffraction Standards (JCPDS).

The morphology was investigated by scanning electron microscopy (SEM) and transmission electron microscopy (TEM). A FEI S-FEG XL30 microscope equipped with energy dispersive X-ray (EDX) spectrometer was used to carry out SEM analysis. EDX allowed to quantify the bulk elemental composition. TEM analysis was performed using a FEI CM12 microscope. The catalysts were suspended in isopropyl alcohol and a few drops deposited on a carbon-coated copper grid.

2.3. Membrane-electrode assemblies (MEAs) preparation

A chemically stabilised melt-extruded Aquivion® membrane (E98-05S), with an equivalent weight (EW) of 980 g eq^{-1} and a thickness of 50 µm, was provided by Solvay Specialty Polymers [34]. This membrane was purified in concentrated sulfuric acid and subsequently in distilled water before its use as separator for the electrodes in a zero-gap configuration PEM electrolysis cell.

The Aquivion® ionomer dispersion (D98-06AS) was employed as catalyst binder and to favour bonding of the catalyst layer to the membrane [34].

A catalyst-coated membrane (CCM) methodology was utilised for the manufacturing of the membrane-electrode assemblies. The technique was based on the spray deposition of the catalyst-ionomer ink, composed by anode or cathode catalysts along with ionomer, directly onto the membrane. Each catalyst-ionomer ink was obtained by weighing fixed quantities of ionomer and catalyst in the proper amounts (Table 1) and dispersing these mixtures in absolute ethanol. Each slurry was mixed in an ultrasonic bath until the total evaporation of

the solvent (the ultrasonic bath reached 50 °C during this procedure). The dry powder was milled in a mortar with a pestle before preparing the final ink for the deposition of the catalyst layers onto the membrane by spray coating. Specific amounts of dry catalyst-ionomer powders were again dispersed in a proper amount of absolute ethanol in an ultrasonic bath and the obtained inks were spray-coated directly onto a membrane sheet kept at 80 °C on a heated metal table.

The composition and catalyst loading of the investigated MEAs are reported in Table 1.

Table 1 Composition and catalyst loading of the investigated MEAs.

MEA code	**Anode**			**Membrane**	**Cathode**	
	IrRuOx catalyst Loading (mg_{Ir+Ru} cm^{-2})	PtCo catalyst Loading (mg_{PtCo} cm^{-2})	Aquivion® D98-06AS ionomer (wt.%)	Aquivion®	Pt/C catalyst loading (mg_{Pt} cm^{-2})	Aquivion® D98-06AS ionomer (wt.%)
Bare	0.3	-	15%	E98-05S	0.1	28%
RC mixed	0.3	0.2	15%	E98-05S	0.1	28%

In the RC mixed MEA, the recombination catalyst was mixed in a proper amount with the anode catalyst and the ionomer to obtain a composite layer made of IrRuOx and PtCo.

CCMs were finally subjected to a hot-pressing procedure (190 °C, 6 kN, 1.5 min) to favour the adhesion of the catalytic layers to the membrane. The temperature selected for the hot pressing procedure was higher than the glass transition temperature of the Aquivion® polymeric membrane (160 °C) [55,56].

A titanium fiber mesh (Bekaert Toko Metal Fiber Co.), characterised by 78% porosity, 20 µm fibre diameter and 0.3 mm thickness, and a carbon cloth (GDL ELAT from ETEK) were used as gas diffusion layers (GDLs), for the anode and cathode, respectively. MEAs were installed in an electrolysis cell housing equipped with a titanium plate at the anode and a

graphite plate at the cathode (Fig. S1). This approach was adopted to avoid possible embrittlement of Ti at the cathode by hydrogen evolution during durability studies. The active area (geometrical electrode area) of the MEAs was 5 cm^2.

2.4. Electrochemical measurements

Before carrying out the polarisation measurements, membrane-electrode assemblies were subjected to a conditioning procedure of 0.05 A cm^{-2} for 24 h to favour MEA hydration and stabilisation of catalysts' oxidation state. Performance and stability of bare and RC mixed MEAs were investigated electrochemically. The PEM electrolysis cell performance was evaluated at different temperatures (30°, 40°, 55°, 60°, 70°, 80° and 90 °C) and under ambient pressure conditions.

Deionised water, milli-Q Integral, Millipore (<0.1 µS), further purified by an ion exchange resin cartridge, was supplied and recirculated (at the same temperature of the cell) by a pump at a flow rate of 4 ml min^{-1} to the anode compartment.

A power supply of 100 A (TDK Genesys™ 25400-MD-3P400) was used to carry out polarisation curves. The current density was gradually increased following an exponential trend. Accordingly, a larger number of data was collected in the low current density range where the effect of the Volmer-Butler equation is prevailing than at high current density where the trend is mainly determined by the Ohmic law. A cut-off voltage of 2.4 V was used.

An Autolab Metrohm potentiostat / galvanostat equipped with a 20 A current booster (Metrohm) and a frequency response analyser (FRA) was used to perform impedance spectroscopy (EIS) studies in the potentiostatic mode. Due to the 20 A upper current limit of the Autolab booster, electrochemical impedance measurements were carried out at 1.5 V and 1.8 V. These conditions are representative of the activation region and the ohmic

drop-controlled region [57]. The frequency was varied from 100 kHz to 100 mHz in the single sine mode. The series resistance R_s was determined from the high frequency intercept on the real axis of the Nyquist plot. The polarisation resistance R_p was determined as difference between the extrapolated low frequency intercept and the high frequency intercept on the real axis.

3. Results and discussion

3.1 Microstructure and morphology of catalysts

Fig. 1 provides information about the structural and morphological properties of the 40 % Pt/C cathode catalyst as provided by XRD and TEM analyses. The inset of Fig.1 reports a TEM micrograph of the cathode catalyst. In spite of the high metal loading on carbon (40% wt.), the Pt/C catalyst consisted of fine metal particles of similar dimensions (3-4 nm) homogeneously dispersed on the carbon support. The TEM analysis was carried out on several portions of the catalyst sample to get a statistically relevant information. No relevant deviations were observed. The diffraction pattern confirmed the occurrence of the typical face centred cubic (fcc) crystallographic structure of platinum (JCPDS card no. 4-802) and the hexagonal crystallographic structure of the carbon support. The XRD pattern (Fig. 1) also showed broad reflection peaks, which were due to the presence of nanosized Pt particles on the carbon support. The average crystallite size of platinum particles was 3.3 nm as estimated by the Debye-Scherrer equation.

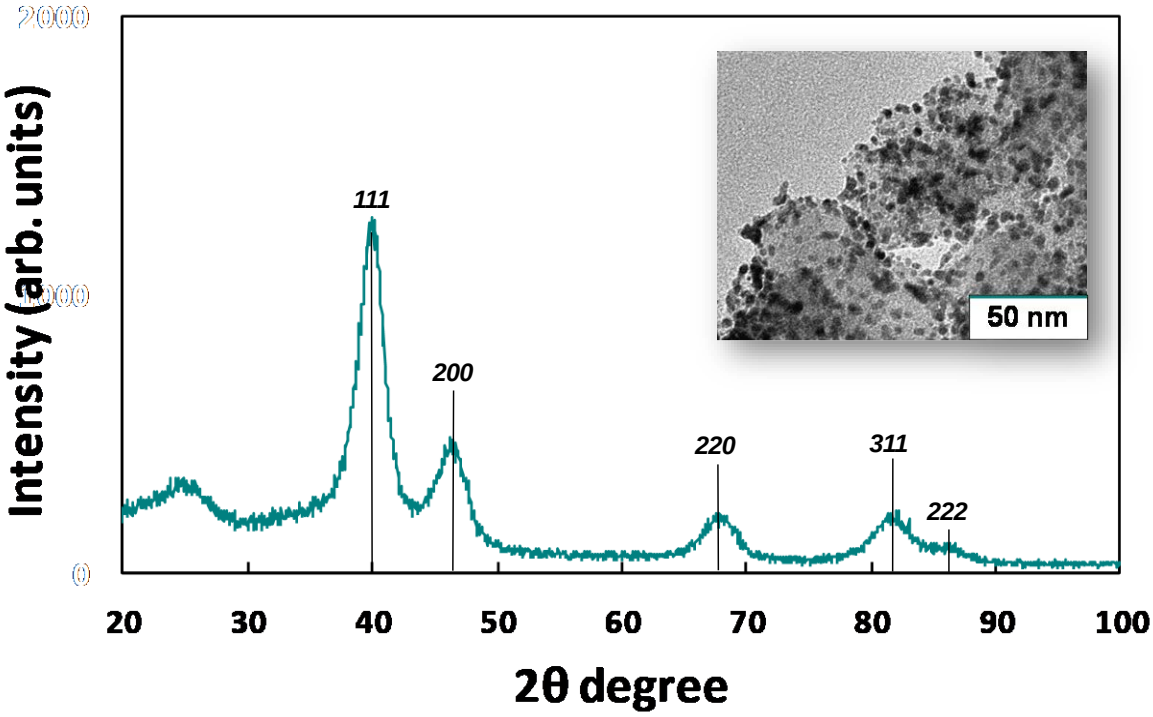

Fig. 1. *X-ray diffraction patterns of the 40 % Pt/C catalyst with face centred cubic Pt structure as indicated by the JCPDS card no. 4-802 (black lines) reflections and carbon hexagonal structure (asterisk), as reference. The inset shows a TEM micrograph of the Pt/C cathode catalyst.*

Fig. 2 shows the X-ray diffraction pattern of the IrRuOx catalyst. The peaks were in this case sharper that those previously observed for the Pt/C. The observed reflections indicated a tetragonal crystallographic structure typical of IrO_2 (JCPDS card no. 15870). The XRD pattern of the catalyst showed a significant shift towards higher Bragg angles with respect to the reference pattern of IrO_2. This effect was ascribed to the lattice contraction in the presence of Ru and the formation of a solid solution of the two metal oxides [58]. The crystallite size, determined according to the Debye-Scherrer equation, was 10 nm for the IrRuOx catalyst.

The morphology of the anode catalyst was also investigated by SEM and TEM analyses. The bulk elemental composition was investigated by means of EDX analysis. These

analyses were carried out on several portions of the sample and, in particular, EDX analysis was made at low magnification (150 x), to get an information statistically relevant for the entire sample. According to the various results, the sample properties appeared highly homogeneous (± 0.2% variation in elemental composition). Fig. S2 reports a representative SEM image and an EDX spectrum of IrRuOx catalyst. The catalyst showed a porous morphology and an atomic ratio Ir:Ru = 73:27 % at. These results were close to the expected nominal ratio ($Ir_{0.7}Ru_{0.3}Ox$). It is pointed out that some unalloyed Ru atoms may have leached-out during the catalyst pre-treatment in acid.

A representative TEM image, reported in the inset of Fig. 2, depicts the occurrence of catalyst agglomerates consisting of fine particles. The TEM micrograph, collected at high magnification (Fig. 2 inset), shows the crystalline lattice of a primary IrRuOX particle. The lattice spacing accounts for the occurrence of a solid solution. TEM analysis highlights the rectangular/squared shape of a large fraction of these nanoparticles; the remaining ones are spherical and smaller. The lattice fringes were used to evaluate the average size of these nanocrystalline domains whose mean value was 10.1 nm. These results were in good agreement with the XRD pattern and the Debye-Scherrer equation's results.

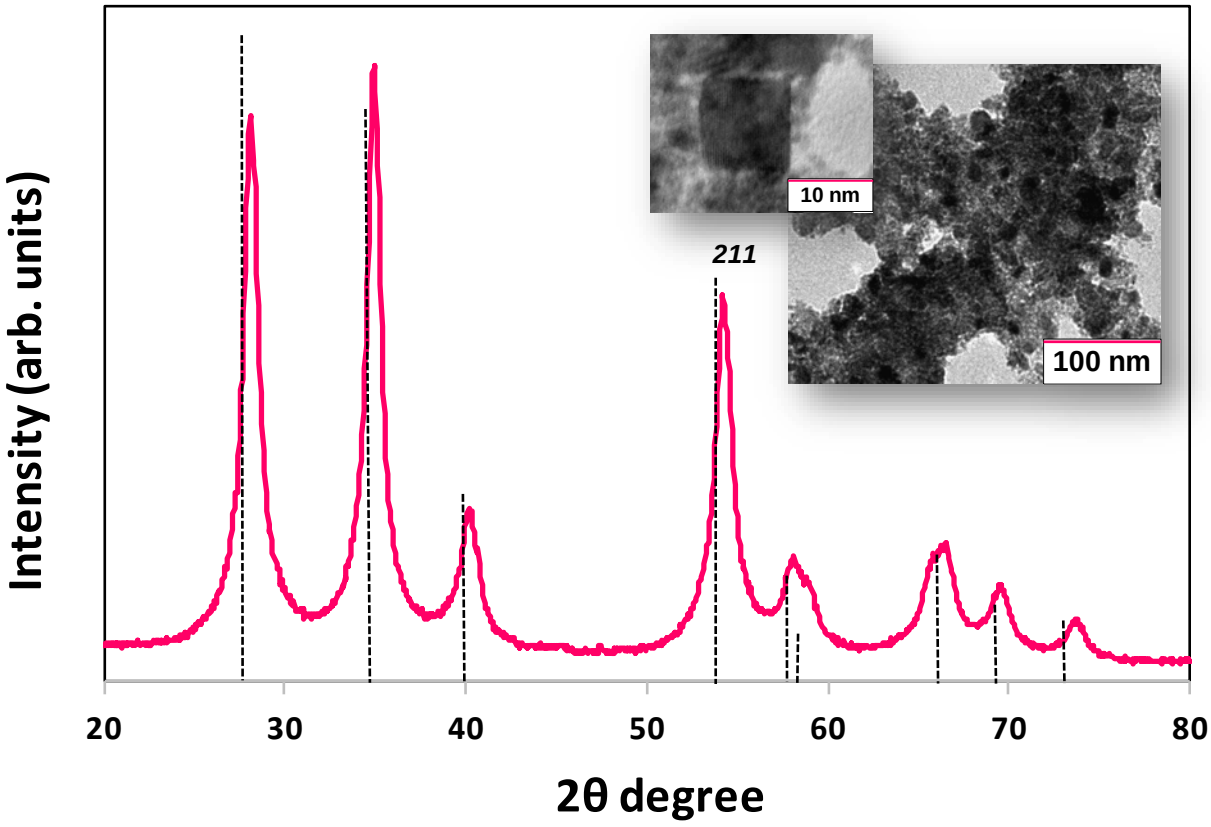

Fig. 2. *X-ray diffraction patterns of IrRuOx (73% at. Ir: 27% at. Ru) along with the tetragonal IrO2, JCPDS card no. 15870, used as a reference (dashed black line). The inset shows TEM micrographs of the anode catalyst at different magnifications and the crystalline lattice of a primary particle.*

Fig. 3 shows some representative results from XRD and TEM analyses carried out on the PtCo recombination catalyst. It is pointed out that these analyses were repeated for several portions of the sample showing no relevant deviations. A face-centered cubic crystallographic structure (JCPDS card no. 4-802) is also observed for this sample. A significant peak shift towards higher Bragg angles, with respect to the diffraction pattern of platinum, is observed for the catalyst. The peak shift is particularly evident for the (220) reflection and, in general, for the peaks at high Bragg angles. This indicates the occurrence of a solid solution of platinum and cobalt forming a metallic alloy. The lattice

constant determined from the 220 reflection (A_{220}=0.3865 nm) indicates a cobalt atomic content of 15 ± 2% in the solid solution as estimated from the Vegard's law. The average crystallite size, as estimated by the Debye-Scherrer equation, is 4 nm; this result confirms a significant reduction of the particle size with respect to our previous Pt-based recombination catalyst (~10 nm) [36].

The morphology of the catalyst was investigated by SEM and TEM analyses. The inset of Fig. 3 shows a TEM micrograph of the recombination catalyst that consists of spherical nanoparticles. There is a relevant agglomeration usually ascribed to the typical morphology of unsupported catalysts. This does not allow estimating correctly the dimension of crystalline domains. The bulk elemental composition of the catalyst was investigated by EDX measurements at low magnification. Fig. S3 reports a SEM image and an EDX spectrum of the PtCo catalyst. The SEM image shows a porous morphology for PtCo. A Pt-Co ratio of 85:15 ±0.2 at. % was obtained without any evidence of impurities.

As discussed in the experimental section, post-synthesis treatments of the PtCo catalyst were carried out. These processes were optimised with respect to a previous work [36] in order to achieve finer PtCo metal particles and possibly a platinum enrichment on the surface. The present approach was consisting in a milder reduction and stronger pre-leaching treatment than those used in a previous work [36]. This allowed to improve the catalyst properties in terms of alloying and dispersion.

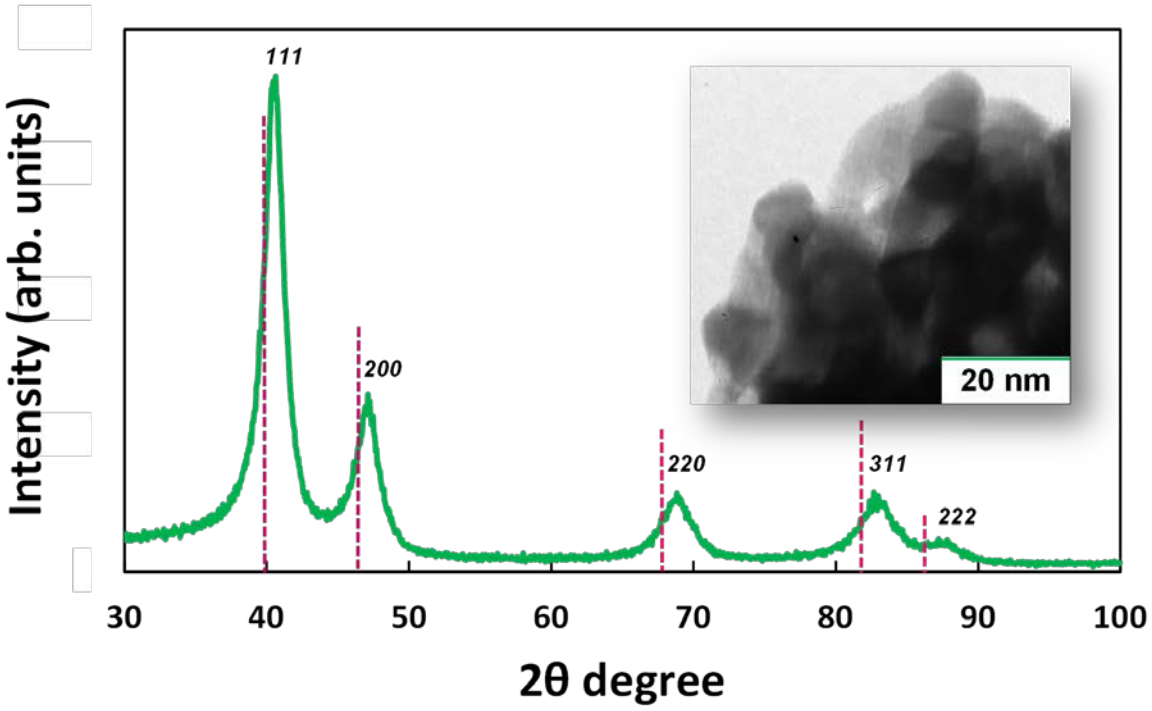

Fig. 3. *X-ray diffraction patterns of the $Pt_{5.6}Co_1$ catalyst and the face centred cubic Pt structure; JCPDS card no. 4-802 was used as reference (dashed pink line). The inset shows a representative TEM micrograph of recombination catalyst.*

3.2 Water electrolysis performance

Fig. 4a shows single cell polarisation curves for the RC mixed MEA containing the PtCo recombination catalyst at the anode. These were collected at different temperatures (from 30 °C to 90 °C) and under ambient pressure conditions. A progressive improvement of cell performance in terms of increase of current density at specific cell voltages was observed with the increase of temperature. As expected, the best performance at high current densities for PEM water electrolysis was achieved at 90 °C. At 90 °C, current densities of 4 A cm^{-2} and 8 A cm^{-2} were recorded at 1.86 V and 2.15 V, respectively.

The impedance behaviour of the electrolysis cell was studied at two different voltages, 1.5 V and 1.8 V, corresponding to activation and ohmic-diffusion control regions, respectively.

At potential values close to the thermoneutral potential, both series and polarisation resistances decreased as the temperature raised (Fig. 4b). The lowest R_s and R_p values at 1.5 V were achieved at 90 °C i.e. 76 mΩ cm^2 and 96 mΩ cm^2, respectively (see inset of Fig. 4b). Impedance spectra recorded at 1.8 V (Fig. 4c) showed a significant decrease of the polarisation resistance, with the lowest value recorded at 90 °C (R_p = 17 mΩ cm^2). No relevant changes in the series resistance values were observed. At 1.8 V, the catalyst contribution to the overall polarisation behaviour is much lower than at 1.5 V. At 1.8 V, the series resistance at 90 °C was about 73 mΩ cm^2, similarly to what observed at 1.5 V.

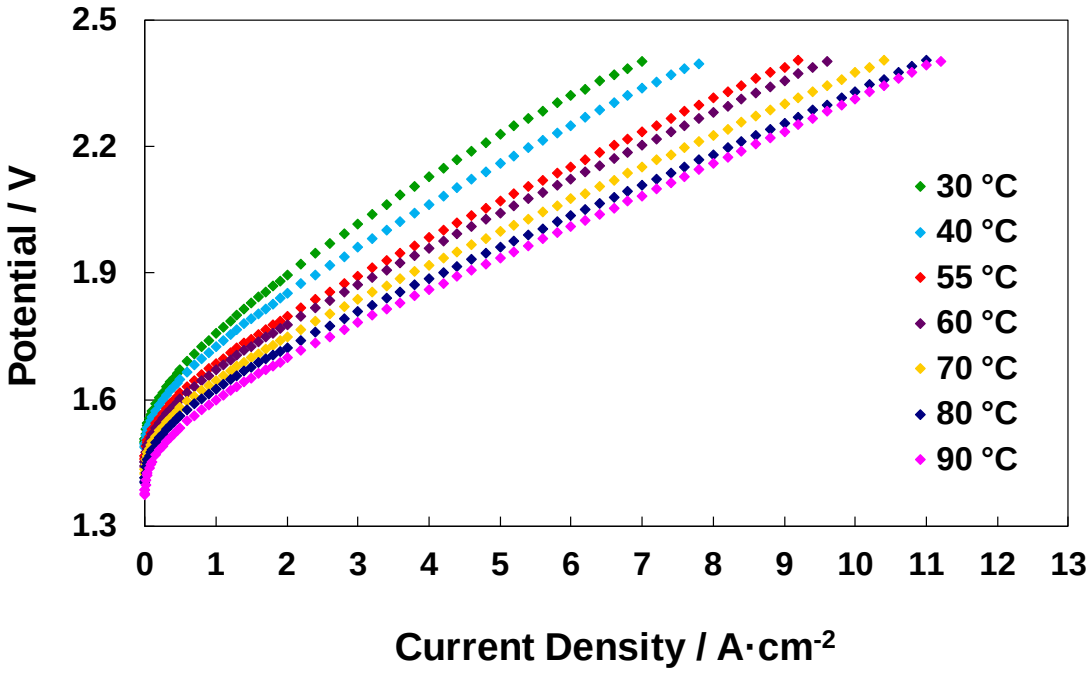

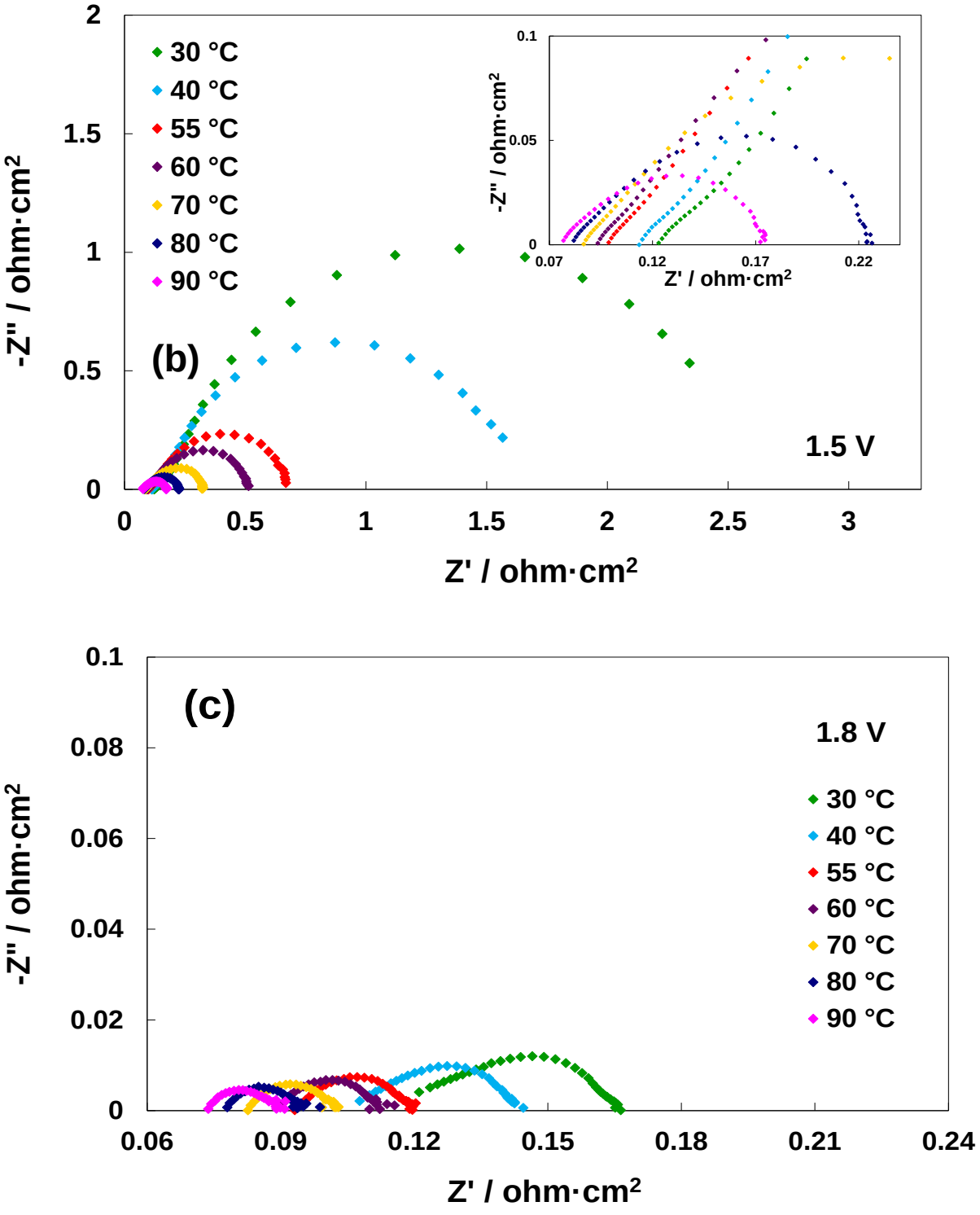

Fig. 4 *Polarisation curves* ***(a)*** *and electrochemical impedance spectra at 1.5 V* ***(b)*** *and 1.8 V* ***(c)*** *at different temperatures for the MEA containing the PtCo recombination catalyst.*

It is interesting to observe that this cell configuration can allow achieving extremely high current densities i.e. larger than 11 A cm^{-2} at 2.4 V. This is made possible by the thin membrane used in this work and the associated low ohmic losses. As shown in a previous work [36], the use of a recombination catalyst of similar type, inside the anode layer, was effective in reducing the hydrogen concentration in the oxygen stream compared to a bare MEA. In general, this approach allows the use of thin membranes while avoiding safety issues with the consequent possibility of achieving extremely high current density.

However, the aim of this work was not regarding electrolysis cell operation at 2.4 V but operation in a potential window around 1.8 V where corrosion issues are much less exacerbated and a good trade-off is obtained between the voltage efficiency and the operating reaction rate.

In the following, we compare the initial (beginning of life - BoL) polarisation curves and ac-impedance spectra of the bare and recombination catalyst-modified MEAs, in a useful potential window, at 80 °C, as reference temperature for PEM electrolysis cells durability assessment.

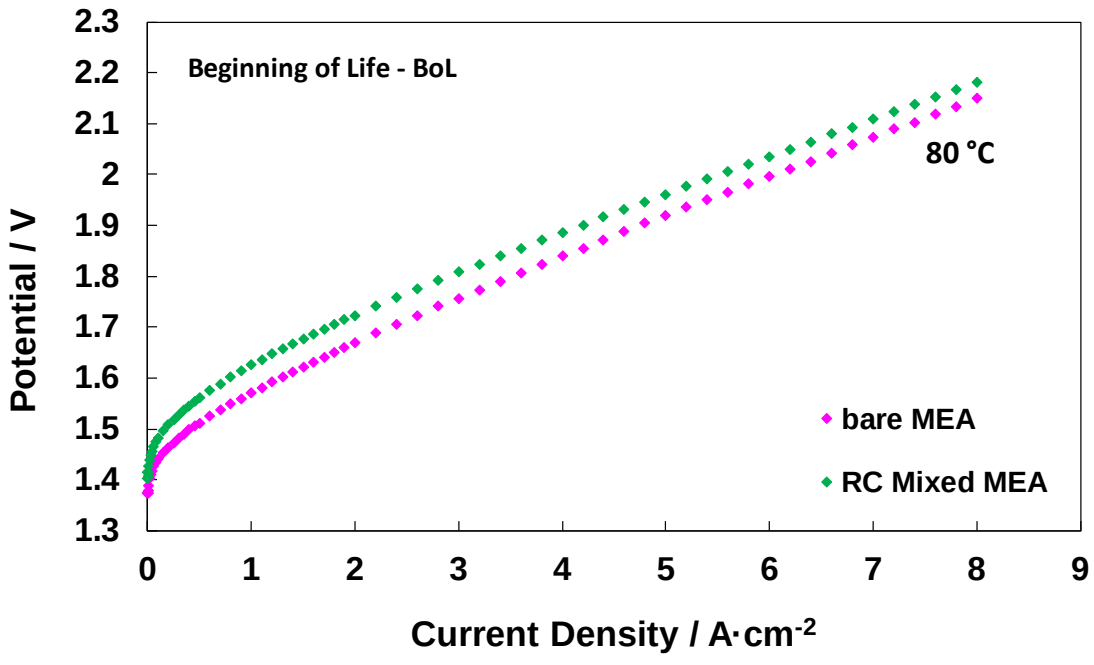

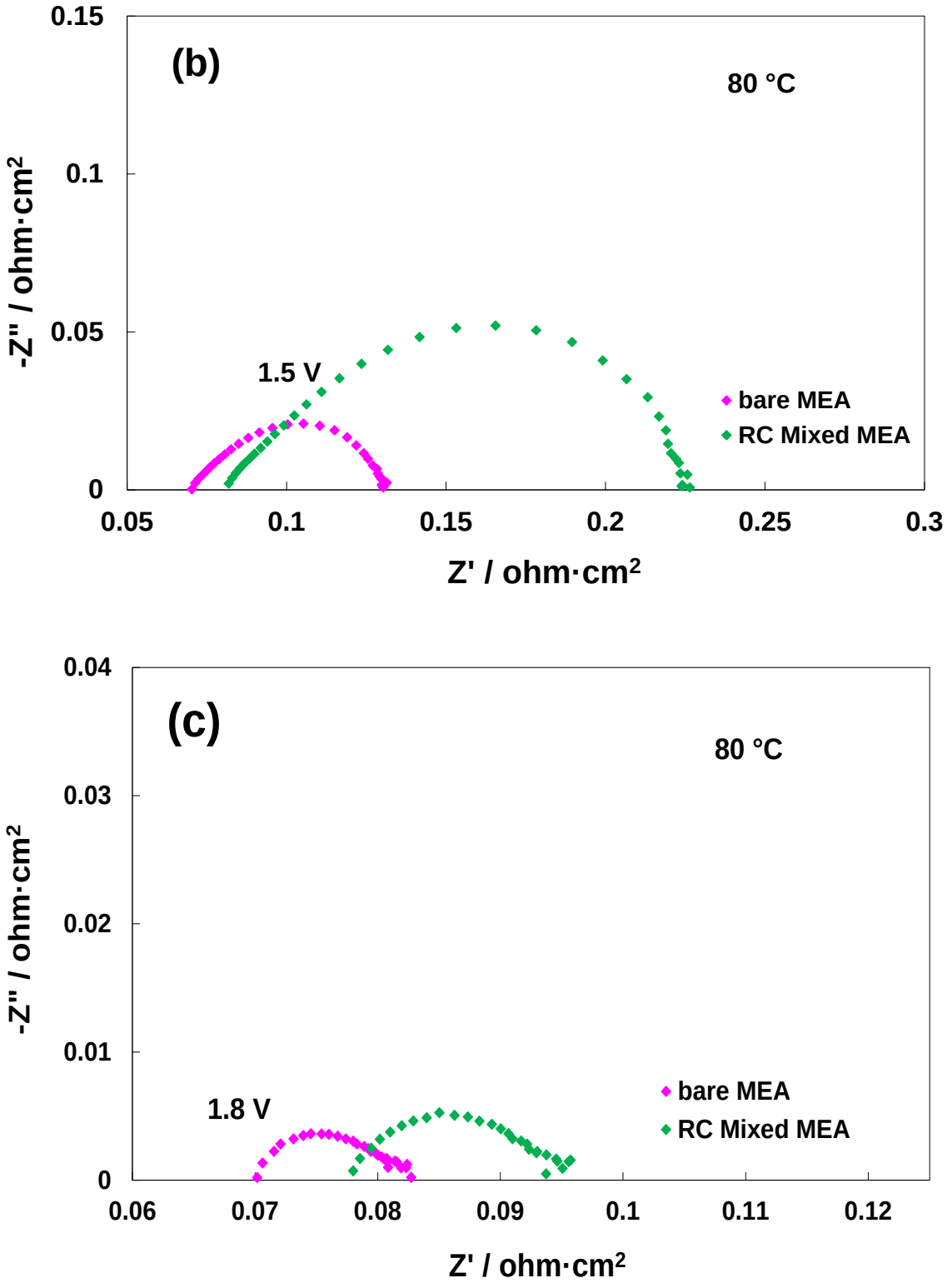

Fig. 5. *Polarisation curves (a) and electrochemical impedance spectra at 1.5 V (b) and 1.8 V (c) at 80 °C of the bare and RC mixed MEAs at beginning of life.*

The comparison of the BoL polarisation curves in Fig 5 indicates a higher cell voltage for the recombination catalyst-based MEA compared to the bare MEA. Ac–impedance spectra show a slightly larger series resistance and, especially, a higher polarisation resistance for the RC mixed MEA. The increase of polarisation resistance may be eventually interpreted in terms of an interference effect caused by the PtCo recombination catalyst on the oxygen evolution process at the IrRuOx catalyst surface. Whereas, the slightly larger series resistance appears to be related to some poisoning of the membrane by the dissolution of unalloyed Co atoms from the PtCo catalyst surface. This may have occurred during the initial MEA conditioning procedure. This may also account for ionomer and IrRuOx catalyst poisoning causing larger polarisation resistance as observed.

The stability is one of the main concerns for PEM electrolysis operation at high current density especially when a low catalyst loading is used [48]. Usually, in a durability study, the cell voltage increases with time more rapidly during the first hundred hours operation than when the cell has already operated for thousand hours. This means that the slope of the durability curve is significantly larger at the beginning of the test; thereafter, the curve tends to flatten. The estimation of the lifetime of an electrolysis system is thus more reliable if the decay rate is assessed after the cell voltage reaches a proper stabilisation. During the first period, the cell experiences some modifications until an equilibrium is reached. These modifications have been investigated in some previous works for bare MEAs [44,59]. As demonstrated in a previous study [48], relevant MEA degradation especially occurs when a low catalyst loading and a high current density are used. This because the turnover frequency for the catalytic sites increases drastically under such conditions [48]. For this reason, it is appropriate to compare the stability of different MEAs with similar catalyst loadings [60,61]. The stability of the bare and RC mixed MEAs have been compared in durability studies of about 3500 h at 80 °C. These consisted of steady

state tests at high current density (4 A cm^{-2}) preceded by a stabilisation procedure at mild current density (1 A cm^{-2}). The experiments specifically consisted of 100 h at 1 A cm^{-2} and 3400 h at 4 A cm^{-2}, as shown in Fig. 6. At the beginning of the durability tests, the cell voltage increased quite rapidly. This result was ascribed to a MEA conditioning effect caused by a possible modification of the oxidation state at the anode catalyst surface and the accumulation of the evolved gases in the catalyst micropores forming a diffusion barrier [62]. The first phenomenon can be caused by the cell switch from OCV (or low anode potential) to a high current density (corresponding to high anode potential). Moreover, the cell voltage for both MEAs increased significantly in the specific short time-span that follows the current density switch from 1 to 4 A cm^{-2}. This result is attributed to the possible occurrence of reversible losses eventually related to mass transport issues or to a change of the oxidation state of the anode catalyst according to the different potential window of operation between 1 and 4 A cm^{-2}. Despite the very low PGM-loading both MEAs showed a reasonable stability especially during the last period of operation.

Interestingly, it is noted that the cell voltage along the durability test is about 30 mV lower for the recombination catalyst-based MEA compared to the bare MEA. This corresponds to about 2-3 % voltage efficiency enhancement.

This is somewhat surprising since the cell voltage was higher for the recombination catalyst-based MEA compared to the bare MEA in the initial polarisation curves. In particular, at 4 A cm^{-2}, the cell voltage for the recombination catalyst-based MEA decreased from 1.88 V in the initial polarisation curve to 1.8 V at the beginning of the steady state durability test. Thus, one may expected that an internal purification, producing a removal of some eventual poisoning species caused by a possible leaching of Co atoms from the surface of PtCo, might have occurred during the first hours of operation at a sustained current density (1 A cm^{-2}). The preliminary MEA conditioning procedure,

preceding the initial polarisation curves, was instead carried out at 0.05 A cm^{-2}; this was probably not sufficient to remove impurities. The larger initial series resistance for the recombination catalyst-based MEA compared to the bare MEA in Fig. 5 may account for the presence of some impurities. These could be related to the leaching of unalloyed Co species. On the other hand, at 4 A cm^{-2}, the bare MEA passed from a cell voltage of about 1.84 V in the polarisation curve to 1.85 V at the beginning of the steady state durability test.

During the steady-state durability test, the recombination catalyst-based MEA did not just recover the initial performance gap versus the bare MEA, as shown in the initial polarisation curves, but it was about 30 mV better. The motivations behind this enhanced performance can be related to two effects. A depolarisation effect of the anode caused by the oxidation of the permeated hydrogen (electrochemical oxidation of the permeated hydrogen at the PtCo sites) or a contribution to the overall oxygen evolution rate produced by the PtCo catalyst added to the IrRuOx layer. An experiment carried out with the PtCo catalyst only at the anode (Fig. S4) showed a much lower performance than the bare MEA but some activity for the oxygen evolution process was observed. Thus, we can not exclude some contribution of the PtCo to the overall oxygen evolution performance. This process may occur in parallel to the chemical recombination process of evolved oxygen and permeated hydrogen into water. The two mechanisms may compete each other making the recombination catalyst less effective than expected. Our previous work [36], showed an effective reduction of the hydrogen concentration in the oxygen stream but the presence of H_2 gas at the anode was not completely eliminated.

The degradation rate was estimated in the durability studies from the best linear fitting excluding the first 100 test hours at 4 A cm^{-2}. This because such region is more affected by reversible voltage losses. The recorded voltage loss for the bare MEA was 20 µV/h at 4

A cm^{-2}. The RC mixed MEA showed a performance decay in the long-term test at 4 A cm^{-2} of 23 µV/h. These are not significantly different considering that the final result may be slightly affected by the number of shut-down and start-up cycles that have inevitably occurred during the 3500 h tests. Moreover, deconvolution of reversible and irreversible losses requires an analysis over a much longer time-scale. However, taking into account the last period, it is observed that the degradation rate for the MEA equipped with the recombination catalyst corresponds to about 9 µV/h in the last 1000 h of operation at 4 A cm^{-2}. The cell voltage vs. time curve appears to flatten considerably after about 1000 h operation.

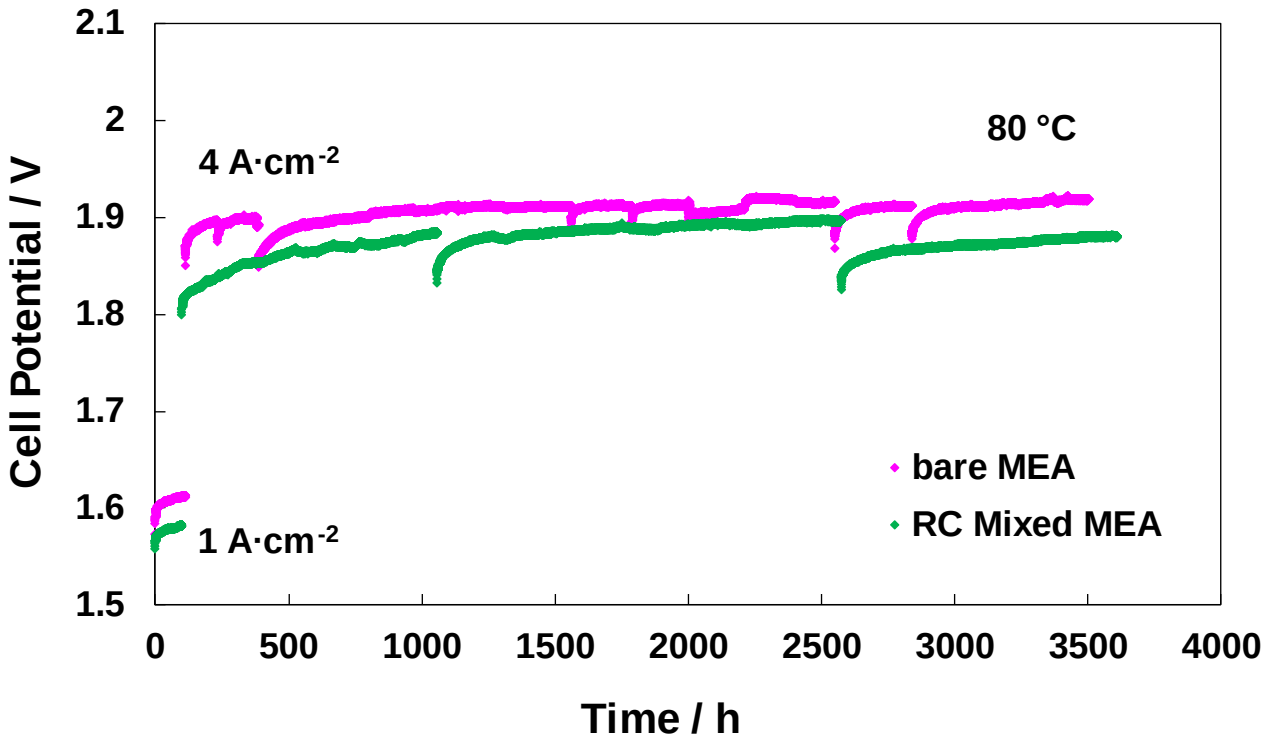

Fig. 6 *Durability test at 1 and 4 A cm^{-2} and 80 °C of the bare and RC mixed MEAs*

In order to understand the modifications that have occurred during the durability tests, both MEAs were electrochemically investigated through polarisation and ac-impedance analyses (Fig. 7). By comparing the end-of-test (EoT) polarisation curves of bare and RC mixed MEAs after a 3500 h steady state operation (Fig. 7a), it is noted that main difference

in performance occurs in the region controlled by ohmic-diffusion phenomena, where the RC Mixed MEA shows a better performance.

Thus, at the end of the test at high current density, the performance of the RC mixed MEA was slightly better than that of the bare MEA (Fig. 7) confirming the evidence observed in the durability studies of a lower cell voltage during the overall test. However, at low current densities the EoT performances were comparable. Thus, the observed enhancement is not probably related to a catalytic improvement but possibly to a better current collection at high current density that is favoured by the additional PtCo catalyst. This effect can not be excluded for such low catalyst loadings where the low catalyst content (0.3 mg_{Ir+Ru} cm^{-2}) is approaching the electronic percolation threshold.

The EoT impedance studies at a potential value (1.5 V), close to the thermoneutral potential, (Fig. 7b) do not show significant differences in series and polarisation resistance for the modified and bare MEAs confirming the evidence of a similar polarisation profile of both MEAs in the activation region.

The impedance spectra recorded at 1.8 V are reported in Fig. 7c. A slight decrease of series resistance (10-15 mΩ cm^2) after 3500 h operation was observed for both MEAs. This may be related to a membrane thinning effect.

A cell voltage of 1.83 V at 4 A cm^{-2} was recorded for the RC mixed MEA after 3500 h durability test. This is slightly lower than that recorded at the beginning of life and it may be due to a membrane thinning effect too caused by prolonged operation.

Moreover, the RC mixed MEA showed lower series resistance in the post-operation analysis compared to the bare MEA (compare Fig. 7c and Fig. 5 c). This has produced a slight increase of performance at high current density in the EoT polarisation curves and a lower cell voltage during the overall durability test. Since the membrane was the same for both MEAs and such difference in cell voltage was observed from the very beginning of

the durability test at 1 A cm^{-2}, the lower cell resistance may not be eventually attributed to a relevant membrane thinning in the case of the recombination catalyst-based MEA. It could be possibly ascribed to a better current collection at such thin anode catalyst layer in the presence of the recombination catalyst as discussed above.

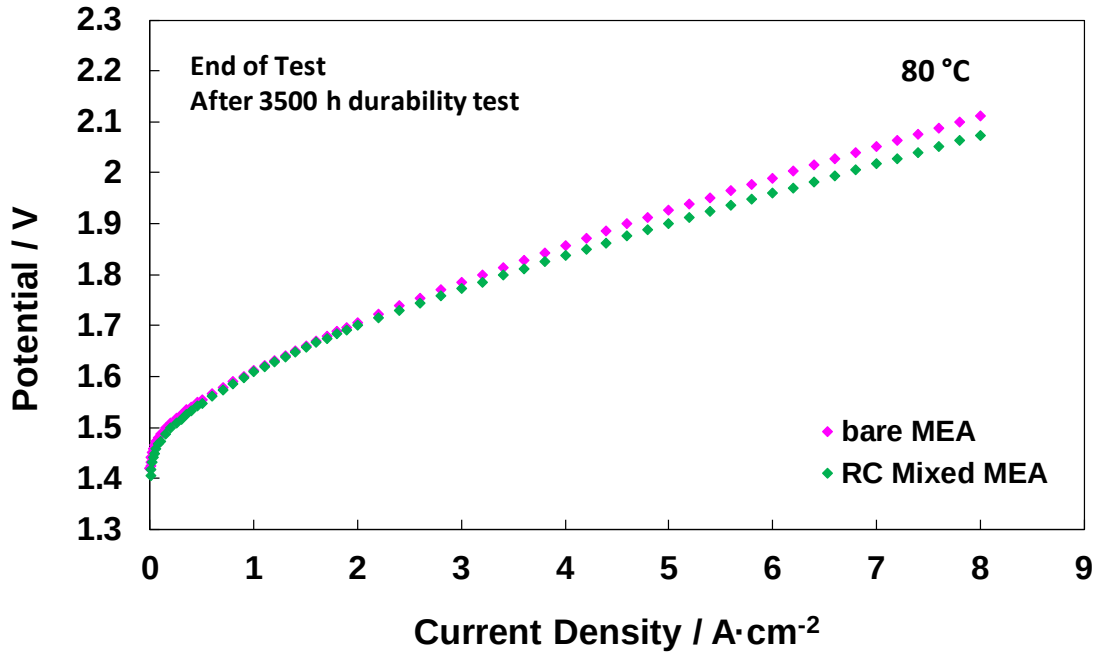

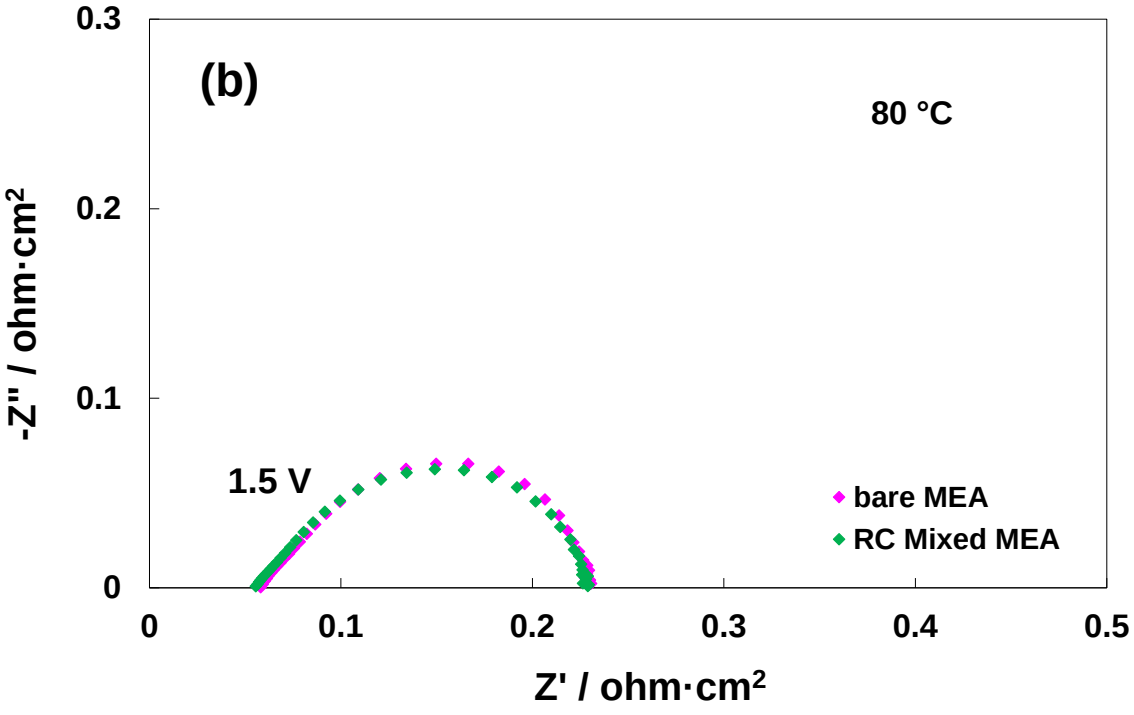

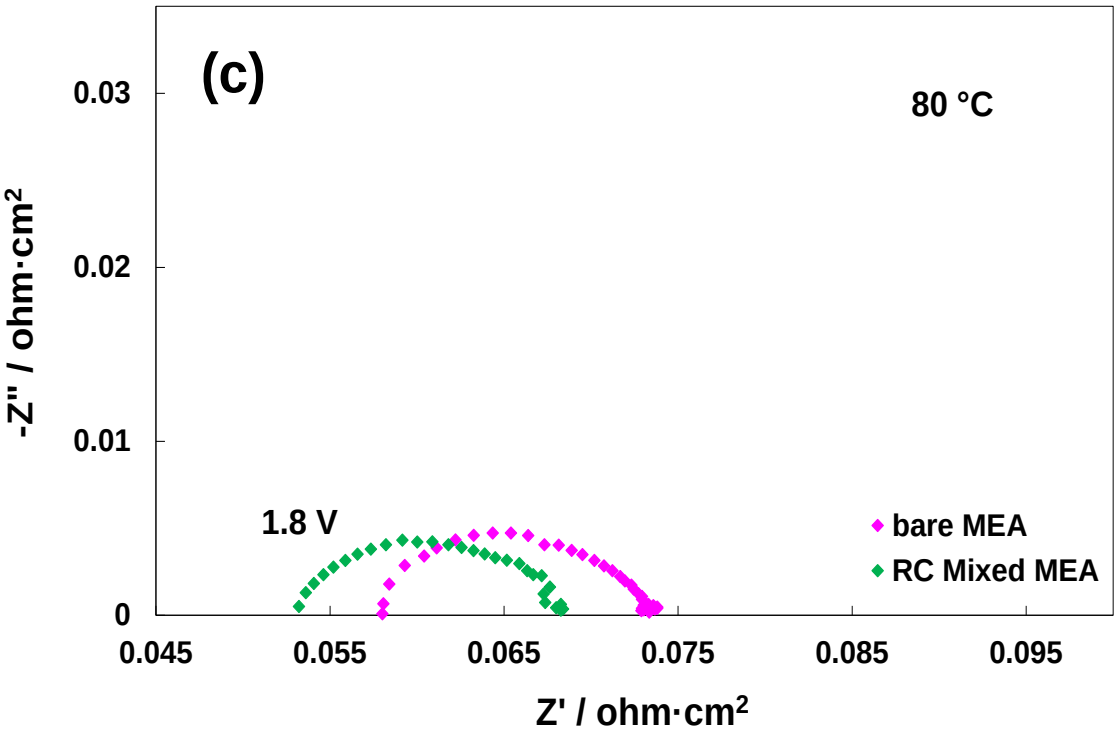

Fig. 7. *Polarisation curves (a) and electrochemical impedance spectra at 1.5 V (b) and 1.8 V (c) at 80 °C after 3500 h durability test of the bare and RC mixed MEAs.*

However, post-operation SEM analysis of the used MEAs confirmed a slight membrane thinning in some regions (Fig. 8). This was slightly more accentuated for the RC-catalyst based MEA (Fig. 8a) than in the bare MEA (Fig. 8b). Both used anode catalyst layers were slightly damaged by MEA dismantling from the cell hardware. In particular, some layers remained attached to the Ti mesh.

a)

Anode ~ 14-15 µm

Membrane ~ 45-50 µm

Cathode ~ 13 µm

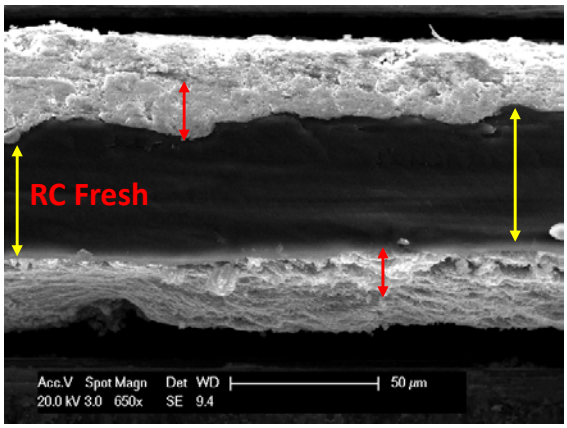

Anode ~ 11-12 µm

Membrane ~ 40-50 µm

Cathode ~ 13 µm

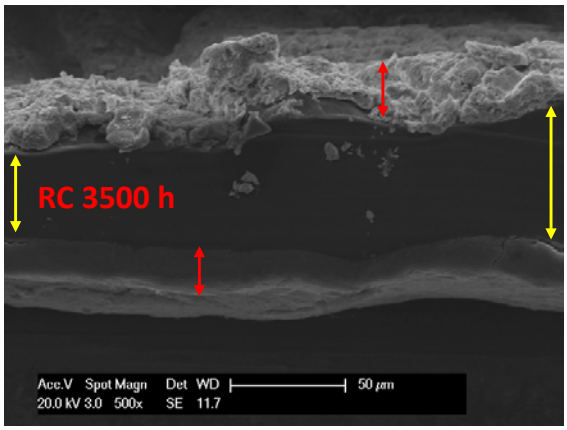

b)

Anode ~ 9-10 µm

Membrane ~ 45-50 µm

Cathode ~ 13 µm

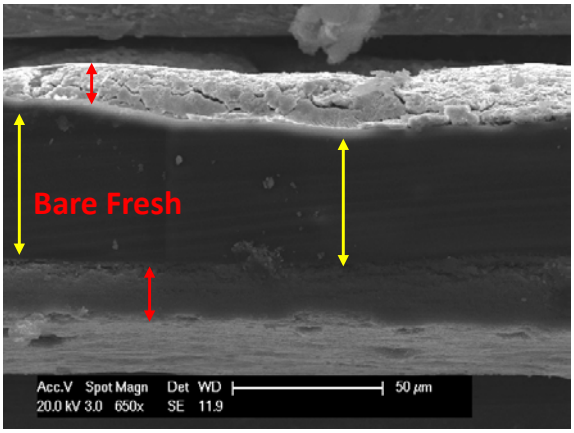

Anode ~ 7-8 µm

Membrane ~ 43-50 µm

Cathode ~ 10-12 µm

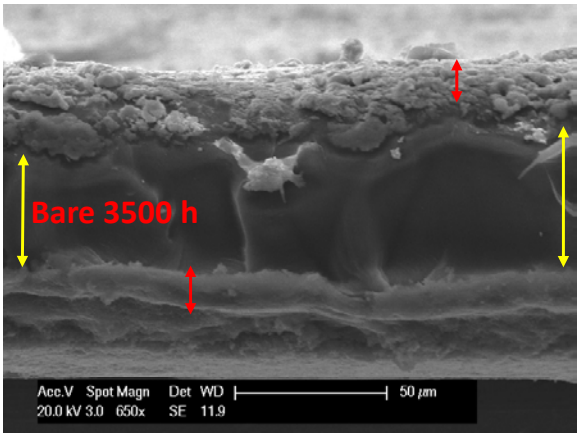

Fig. 8 *SEM analyses of MEA cross-sections before (fresh) and after 3500 h (used) durability test for the RC mixed (a) and bare (b) MEAs; the anode layer is shown on the top of membrane for all MEAs.*

Another important information, provided by ac-impedance analysis, regards the polarisation resistance variation after prolonged electrolysis operation. At 1.5 V, the charge transfer resistance (Rp) in the EIS spectra of the bare MEA enlarged significantly after the durability test while the one for the RC mixed MEA remained almost unchanged (compare Fig. 5b and Fig. 7b). For the RC mixed MEA, an EoT polarisation resistance of 15 mOhm cm^2 at 1.8 V was observed (Fig. 7c). This is comparable to what was recorded at 80 °C at the beginning of life for the same MEA (about 18 mOhm cm^2); similarly at 1.5 V, the polarisation resistance for the RC mixed MEA, after the durability test (EoT), was 0.18 Ohm cm^2 compared to 0.2 Ohm cm^2 at the beginning of life (compare Fig. 5b and Fig. 7b). At 1.8 V, the polarisation resistance for the bare MEA increased only slightly from about 0.12 Ohm cm^2 to 0.15 Ohm cm^2 after the 3500 h durability test (compare Fig. 5c and Fig. 7c).

Taking into account the information obtained from the impedance spectra at 1.5 V (activation region), some catalyst degradation may have occurred for the bare MEA. However, the observed differences are much smaller at 1.8 V. This condition refers to the cell operation at high current density. Accordingly, one may say that the catalysts degradation has a lower impact on the polarisation resistance when a proper overpotential (e.g. 300 mV vs. the thermoneutral potential) is applied. Thus, the present tests of 3500 h do not reveal significant polarisation losses at high current density. Some catalyst restructuring during prolonged electrolysis operation or a change of the interface extension between the catalyst and the ionomer, as observed previously [44], could have occurred. It appears clear in the durability tests that there is a rapid increase of cell voltage in the first

thousand hours thereafter the curves tend to flatten especially at the end of test.

A morphology investigation was thus carried out for the catalytic layers of the fresh MEAs and the MEAs that had operated for 3500 h at high current density (Figs. 9-10). The SEM analysis (Fig. 9) showed for the RC-based anode the occurrence of bright spherical agglomerates (100-200 nm) formed of fine particles (<10 nm), associated to the recombination catalyst. These were more evident in the used sample compared to the fresh MEA (Fig. 9a-b). The IrRuOx morphology consisted of largely agglomerated nanosized particles (~10 nm) with dark colour at high magnification (Fig. 9a-b, Fig.10 a-b). These did not appear to change significantly with the durability test in both MEAs (Fig. 9a-b, Fig.10 a-b). After prolonged operation, the cathode catalysts also showed similar dispersion of nanosized particles in the used MEAs compared to the fresh samples without relevant sintering (Fig. 9c-d, Fig. 10c-d).

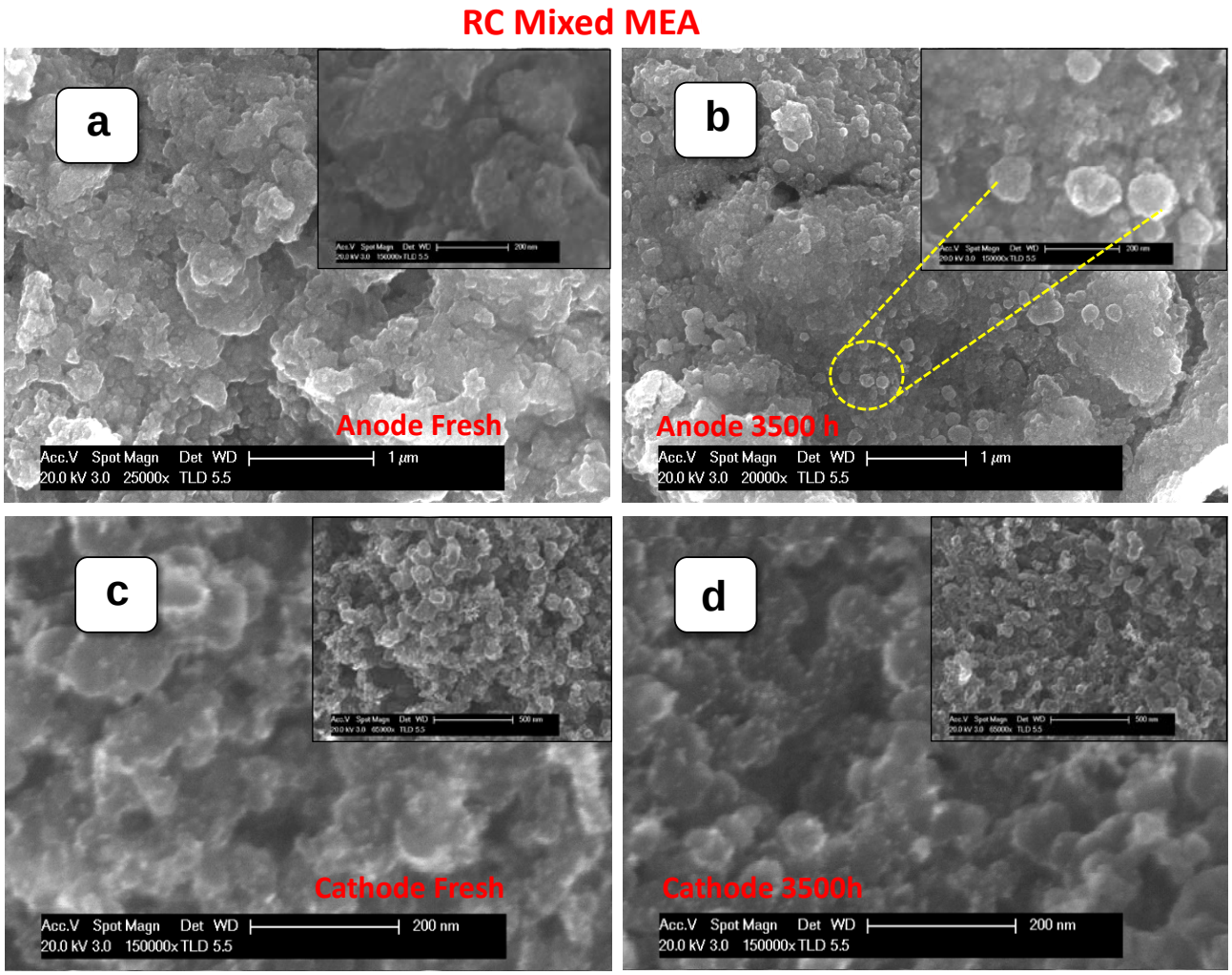

Fig. 9 *Morphology of RC mixed MEA before (fresh) and after 3500 h (used) durability test. The SEM images refer to a) fresh and b) used anodes, c) fresh and d) used cathodes. SEM micrographs at higher and lower magnification are reported in the insets, for anodes and cathodes, respectively.*

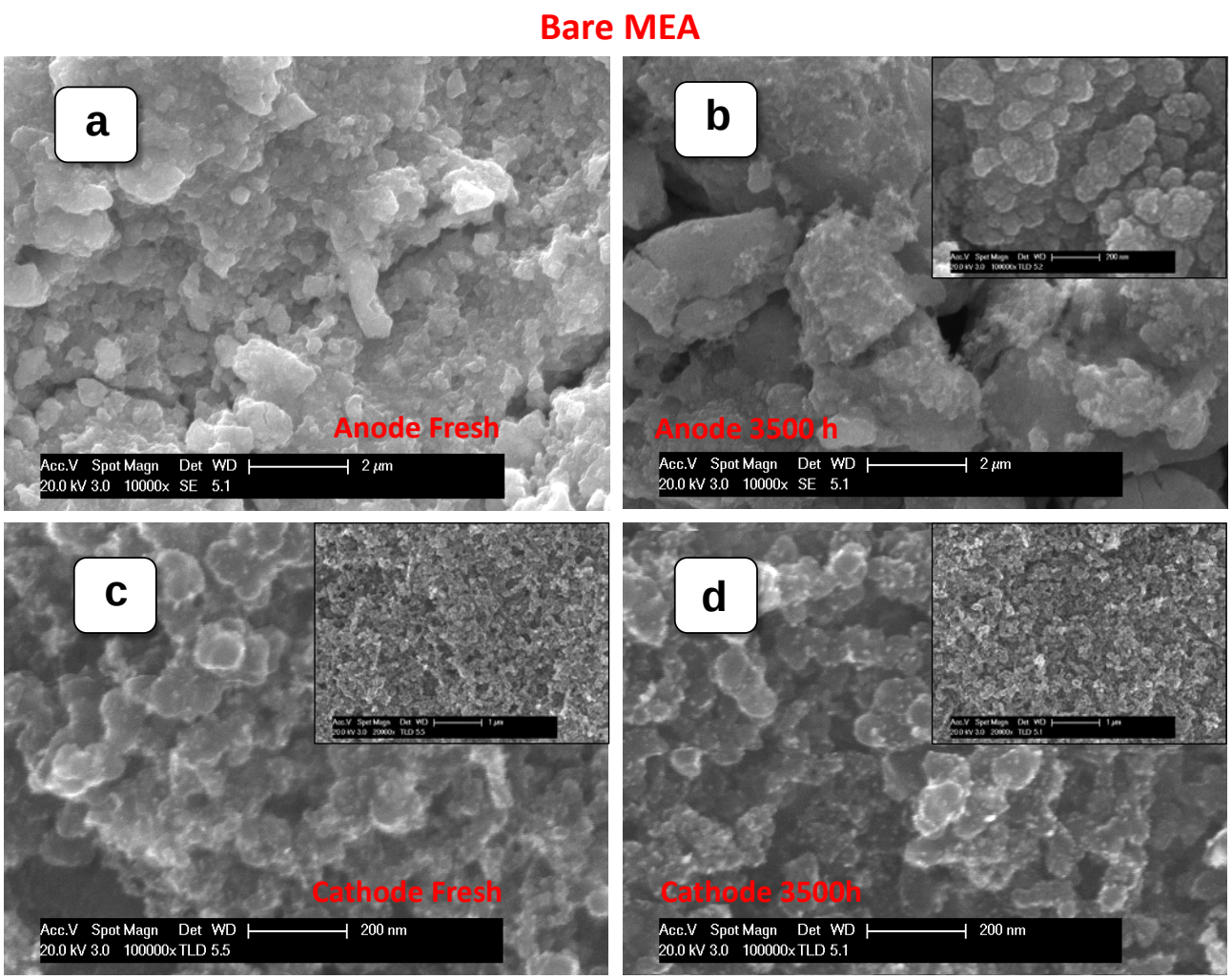

Fig. 10 *Morphology of bare MEAs before (fresh) and after 3500 h (used) durability test. The SEM images refer to samples a) fresh and b) used anodes, c) fresh and d) used cathodes. SEM micrographs at high and low magnification are reported in the insets for anodes and cathodes, respectively.*

Accordingly, there is no evident modification of the catalytic layers morphology after the durability tests.

Finally, it is clarified that some recoverable losses occurring during the durability test are not probably observed in the final polarisation curves since the cell load was switched to the open-circuit voltage (OCV) before carrying out the EoT cell polarisation. The rest interval at OCV may have allowed the gases accumulated in the catalyst micropores to escape leaving these empty. In parallel, a possible variation of the oxidation state on the surface for the anode catalyst may have also occurred. This has probably brought the catalytic activity at the surface to a level similar to that at the beginning of life. It is evident

that, at the end of the durability test, for the RC-based MEA, the cell voltage was 1.88 V at 4 A cm^{-2} in Fig. 6 whereas in the following polarisation curve it was 1.83 V at the same current density. Thus, the rest interval at OCV appears beneficial for the cell performance. This is also evident in Fig. 6; when some cell shut-down and start-up cycles have inevitably occurred during 3500 h operation, the cell voltage was always lower after the switch from OCV to 4 A cm^{-2} compared to the continuous operation. The durability test shows for the recombination catalyst-based MEA a good capability of operating stably with a voltage efficiency of about 80 % vs. the high heating value (HHV) of hydrogen [63] at a high current density of 4 A cm^{-2} (see supplementary data). This appears promising also in relation to the enhanced safety characteristics [36].

4. Conclusions

A recombination catalyst-based membrane-electrode assembly was developed. This consisted of a thin PFSA membrane, an unsupported IrRuOx (70% at. Ir: 30% at. Ru) electrocatalyst, a 40 wt.% Pt on Ketjenblack® carbon (Pt/C) supported cathode catalyst and an unsupported Pt-Co alloy (85:15 at. %) recombination catalyst. The latter was synthesized by means of a sulphite-complex route and its properties were properly optimised for electrolysis operation. In particular, the thermal treatments and pre-leaching processes were optimised in order to obtain a stable solid solution characterised by high degree of alloying. The PtCo catalyst was mixed with the anode catalyst forming a composite anode layer to carry out two relevant catalytic functions i.e. oxygen evolution and oxidation of the permeated hydrogen. The latter process is needed to bring down the concentration of H_2 in the oxygen stream in the presence of thin membranes. This is particularly relevant for safety reasons during high differential pressure operation.

The durability properties of the recombination catalyst-based MEA were investigated for the first time at high current density (4 A cm^{-2}) showing very low performance losses. The cell voltage increased more rapidly at the beginning of the test but the durability curve showed a consistent flattening after 3500 h operation (decay rate of 9 µV/h in the last 1000 h). The cell voltage of the recombination catalyst-based MEA was about 30 mV lower than that of the bare MEA subjected to a similar durability test.

A comparison of the initial and end of test (3500 h) polarisation curves for the recombination catalyst-based MEA showed essentially similar cell voltages at 4 A cm^{-2}. The end of test cell voltage for the recombination catalyst based MEA was 1.83 V in the polarisation curve and 1.88 V in the durability test indicating a beneficial effect produced by the rest interval at OCV. This was also evident in the durability test when some cell shut-down and start-up cycles have inevitably occurred during 3500 h operation.

A post-operation SEM analysis showed a small membrane thinning but no relevant morphology modifications for the catalytic layer. The recombination catalyst nanoparticles appeared just slightly more agglomerated.

The objective of the present study was also to evaluate operation at high current density (4 A cm^{-2}) for PEM electrolysis MEAs consisting of low catalyst loadings (0.4-0.6 mg_{MEA} PGM cm^{-2}). These aspects are both relevant for decreasing the capital costs of a PEM electrolyser. In parallel, the stable voltage efficiency of 80% vs. the high heating value (HHV) of hydrogen at 4 A cm^{-2}, achieved in this study, can allow decreasing operating expenditures.

Another important result of this study was the evidence of a lower cell voltage versus time for the recombination-catalyst based MEA compared to the bare MEA.

In conclusion, the use of an MEA-integrated PtCo catalyst may allow electrolysers to operate in the presence of thin membranes at very high current densities with a reduction of safety issues without compromising the cell durability.

Acknowledgements

CNR-ITAE authors acknowledge the financial support from the NEPTUNE project. This project has received funding from Fuel Cells and Hydrogen 2 Joint Undertaking under grant agreement N. 779540. This Joint Undertaking receives support from the European Union's Horizon 2020 research and innovation programme and Hydrogen Europe and Hydrogen Europe Research. The authors also thank Solvay Specialty Polymers for supplying the Aquivion® membrane and ionomer.

References

[1] Kang J-N, Wei Y-M, Liu L-C, Han R, Yu B-Y, Wang J-W. Energy systems for climate change mitigation: A systematic review. Appl Energy 2020;263:114602. https://doi.org/10.1016/J.APENERGY.2020.114602.

[2] McPherson M, Johnson N, Strubegger M. The role of electricity storage and hydrogen technologies in enabling global low-carbon energy transitions. Appl Energy 2018;216:649–61. https://doi.org/10.1016/J.APENERGY.2018.02.110.

[3] Carmo M, Fritz DL, Mergel J, Stolten D. A comprehensive review on PEM water electrolysis. Int J Hydrogen Energy 2013;38:4901–34. https://doi.org/10.1016/j.ijhydene.2013.01.151.

[4] Robinius M, Raje T, Nykamp S, Rott T, Müller M, Grube T, et al. Power-to-Gas: Electrolyzers as an alternative to network expansion – An example from a distribution system operator. Appl Energy 2018;210:182–97. https://doi.org/10.1016/J.APENERGY.2017.10.117.

[5] Bensmann B, Hanke-Rauschenbach R, Müller-Syring G, Henel M, Sundmacher K. Optimal configuration and pressure levels of electrolyzer plants in context of power-to-gas applications. Appl Energy 2016;167:107–24. https://doi.org/10.1016/J.APENERGY.2016.01.038.

[6] Millet P, Mbemba N, Grigoriev SA, Fateev VN, Aukauloo A, Etiévant C. Electrochemical performances of PEM water electrolysis cells and perspectives. Int J Hydrogen Energy 2011;36:4134–42. https://doi.org/10.1016/J.IJHYDENE.2010.06.105.

[7] Moseley PT, Garche J. Electrochemical Energy Storage for Renewable Sources and Grid Balancing. 2014. 2015 Elsevier B.V. https://doi.org/10.1016/C2012-0-01253-7.

[8] Böhm H, Zauner A, Rosenfeld DC, Tichler R. Projecting cost development for future large-scale power-to-gas implementations by scaling effects. Appl Energy 2020;264:114780. https://doi.org/10.1016/J.APENERGY.2020.114780.

[9] Apostolou D. Optimisation of a hydrogen production – storage – re-powering system participating in electricity and transportation markets. A case study for Denmark. Appl Energy 2020;265:114800. https://doi.org/10.1016/J.APENERGY.2020.114800.

[10] Kato M, Maezawa S, Sato K, Oguro K. Polymer-electrolyte water electrolysis. Appl Energy 1998;59:261–71. https://doi.org/10.1016/S0306-2619(98)00014-2.

[11] Troncoso E, Newborough M. Electrolysers as a load management mechanism for power systems with wind power and zero-carbon thermal power plant. Appl Energy 2010;87:1–15. https://doi.org/10.1016/J.APENERGY.2009.04.006.

[12] Lettenmeier P, Wang R, Abouatallah R, Helmly S, Morawietz T, Hiesgen R, et al. Durable Membrane Electrode Assemblies for Proton Exchange Membrane Electrolyzer Systems Operating at High Current Densities. Electrochim Acta, 2016;210:502–11. https://doi.org/10.1016/j.ELECTACTA.2016.04.164

[13] Cinti G, Baldinelli A, Di Michele A, Desideri U. Integration of Solid Oxide Electrolyzer and Fischer-Tropsch: A sustainable pathway for synthetic fuel. Appl Energy 2016;162:308–20. https://doi.org/10.1016/J.APENERGY.2015.10.053.

[14] Millet P, Ngameni R, Grigoriev SA, Mbemba N, Brisset F, Ranjbari A, et al. PEM water electrolyzers: From electrocatalysis to stack development. Int J Hydrogen Energy 2010;35:5043–52. https://doi.org/10.1016/J.IJHYDENE.2009.09.015.

[15] Reuß M, Grube T, Robinius M, Preuster P, Wasserscheid P, Stolten D. Seasonal storage and alternative carriers: A flexible hydrogen supply chain model. Appl Energy 2017;200:290–302. https://doi.org/10.1016/J.APENERGY.2017.05.050.

[16] van Leeuwen C, Mulder M. Power-to-gas in electricity markets dominated by renewables. Appl Energy 2018;232:258–72. https://doi.org/10.1016/J.APENERGY.2018.09.217.

[17] Tjarks G, Gibelhaus A, Lanzerath F, Müller M, Bardow A, Stolten D. Energetically-optimal PEM electrolyzer pressure in power-to-gas plants. Appl Energy 2018;218:192–8. https://doi.org/10.1016/J.APENERGY.2018.02.155.

[18] Bareiß K, de la Rua C, Möckl M, Hamacher T. Life cycle assessment of hydrogen from proton exchange membrane water electrolysis in future energy systems. Appl Energy 2019;237:862–72. https://doi.org/10.1016/J.APENERGY.2019.01.001.

[19] Bensmann B, Hanke-Rauschenbach R, Müller-Syring G, Henel M, Sundmacher K. Optimal configuration and pressure levels of electrolyzer plants in context of power-to-gas applications. Appl Energy 2016;167:107–24. https://doi.org/10.1016/J.APENERGY.2016.01.038.

[20] Giancola S, Zatoń M, Reyes-Carmona Á, Dupont M, Donnadio A, Cavaliere S, et al. Composite short side chain PFSA membranes for PEM water electrolysis. J Memb Sci 2019;570–571:69–76. https://doi.org/10.1016/j.memsci.2018.09.063.

[21] Bessarabov D. Membranes with recombination catalyst for hydrogen crossover reduction: Water electrolysis. ECS Trans 2018;85:17–25. https://doi.org/10.1149/08511.0017ecst.

[22] Gago AS, Bürkle J, Lettenmeier P, Morawietz T, Handl M, Hiesgen R, et al. Degradation of Proton Exchange Membrane (PEM) Electrolysis: The Influence of Current Density. ECS Trans 2018;86:695–700. https://doi.org/10.1149/08613.0695ecst.

[23] Kalinnikov AA, Grigoriev SA, Bessarabov DG. Nonequilibrium poroelectroelastic theory for polymer electrolytes under conditions of water electrolysis. Int J Hydrogen Energy 2019;44:7889–904. https://doi.org/10.1016/J.IJHYDENE.2019.02.025.

[24] Briguglio N, Brunaccini G, Siracusano S, Randazzo N, Dispenza G, Ferraro M, et al. Design and testing of a compact PEM electrolyzer system. Int J Hydrogen Energy 2013;38:11519–29. https://doi.org/10.1016/j.ijhydene.2013.04.091.

[25] Grigoriev SA, Millet P, Korobtsev SV, Porembskiy VI, Pepic M, Etievant C, et al. Hydrogen safety aspects related to high-pressure polymer electrolyte membrane water electrolysis. Int J Hydrogen Energy 2009;34:5986–91. https://doi.org/10.1016/J.IJHYDENE.2009.01.047.

[26] Briguglio N, Pantò F, Siracusano S, Aricò AS. Enhanced performance of a PtCo recombination catalyst for reducing the H_2 concentration in the O_2 stream of a PEM

electrolysis cell in the presence of a thin membrane and a high differential pressure. Electrochim Acta 2020;344:136153-57. https://doi.org/10.1016/j.electacta.2020.136153.

[27] Trinke P, Bensmann B, Reichstein S, Hanke-Rauschenbach R, Sundmacher K. Hydrogen permeation in PEM electrolyzer cells operated at asymmetric pressure conditions. J Electrochem Soc 2016;163:F3164–70. https://doi.org/10.1149/2.0221611jes.

[28] Cossar E, Oyarce Barnett A, Seland F, Baranova EA. The Performance of Nickel and Nickel-Iron Catalysts Evaluated As Anodes in Anion Exchange Membrane Water Electrolysis. Catalysts 2019;9:814. https://doi.org/10.3390/catal9100814.

[29] Lickert T, Kiermaier ML, Bromberger K, Ghinaiya J, Metz S, Fallisch A, et al. On the influence of the anodic porous transport layer on PEM electrolysis performance at high current densities. Int J Hydrogen Energy 2020;45:6047–58. https://doi.org/10.1016/J.IJHYDENE.2019.12.204.

[30] Nouri-Khorasani A, Tabu Ojong E, Smolinka T, Wilkinson DP. Model of oxygen bubbles and performance impact in the porous transport layer of PEM water electrolysis cells. Int J Hydrogen Energy 2017;42:28665–80. https://doi.org/10.1016/J.IJHYDENE.2017.09.167.

[31] Grigoriev SA, Porembskiy VI, Korobtsev SV, Fateev VN, Auprêtre F, Millet P. High-pressure PEM water electrolysis and corresponding safety issues. Int J Hydrogen Energy 2011;36:2721–8. https://doi.org/10.1016/j.ijhydene.2010.03.058.

[32] Choe S, Lee B-S, Cho MK, Kim H-J, Henkensmeier D, Yoo SJ, et al. Electrodeposited IrO2/Ti electrodes as durable and cost-effective anodes in high-temperature polymer-membrane-electrolyte water electrolyzers. Appl Catal B Environ 2018;226:289–94. https://doi.org/10.1016/J.APCATB.2017.12.037.

[33] Schröder V, Emonts B, Janßen H, Schulze H-P. Explosion limits of hydrogen/oxygen mixtures at initial pressures up to 200 bar. Chem Eng Technol 2004;27:847–51. https://doi.org/10.1002/ceat.200403174.

[34] Siracusano S, Oldani C, Navarra MA, Tonella S, Mazzapioda L, Briguglio N, et al. Chemically stabilised extruded and recast short side chain Aquivion® proton exchange membranes for high current density operation in water electrolysis. J Memb Sci 2019;578:136–48. https://doi.org/10.1016/j.memsci.2019.02.021.

[35] Papakonstantinou G, Sundmacher K. H_2 permeation through N117 and its consumption by IrOx in PEM water electrolyzers. Electrochem Commun 2019;108:106578. https://doi.org/10.1016/j.elecom.2019.106578.

[36] Briguglio N, Siracusano S, Bonura G, Sebastián D, Aricò AS. Flammability reduction in a pressurised water electrolyser based on a thin polymer electrolyte membrane through a Pt-alloy catalytic approach. Appl Catal B Environ 2019;246:254–65. https://doi.org/10.1016/j.apcatb.2018.12.079.

[37] Trinke P, Bensmann B, Hanke-Rauschenbach R. Current density effect on hydrogen permeation in PEM water electrolyzers. Int J Hydrogen Energy 2017;42:14355–66. https://doi.org/10.1016/j.ijhydene.2017.03.231.

[38] Watanabe M, Uchida H, Emori M. Analyses of self-humidification and suppression of gas crossover in Pt-dispersed polymer electrolyte membranes for fuel cells. J Electrochem Soc 1998;145:1137–41. https://doi.org/10.1149/1.1838429.

[39] Aricò AS, Siracusano S, Briguglio N, Baglio V, Di Blasi A, Antonucci V. Polymer electrolyte membrane water electrolysis: Status of technologies and potential applications in combination with renewable power sources. J Appl Electrochem 2013;43:107–18. https://doi.org/10.1007/s10800-012-0490-5.

[40] Shepelin V, Koshmanov D, Chepelin E. Catalyst for recombination of hydrogen and oxygen in confined spaces under high concentrations of hydrogen. Nucl Technol 2012;178:29–38. https://doi.org/10.13182/NT12-A13545.

[41] Klose C, Trinke P, Böhm T, Bensmann B, Vierrath S, Hanke-Rauschenbach R, et al. Membrane interlayer with Pt recombination particles for reduction of the anodic hydrogen content in PEM water electrolysis. J Electrochem Soc 2018;165:F1271–7. https://doi.org/10.1149/2.1241814jes.

[42] Abdalla S, Al-Marzouki F, Obaid A. Safety considerations during production and consumption of hydrogen using proton exchange membrane electrolysis. Journal of Renewable and Sustainable Energy 2017;9:013101. https://doi.org/10.1063/1.4973859.

[43] Siracusano S, Van Dijk N, Backhouse R, Merlo L, Baglio V, Aricò AS. Degradation issues of PEM electrolysis MEAs. Renew Energy 2018;123:52–7. https://doi.org/10.1016/j.renene.2018.02.024.

[44] Siracusano S, Baglio V, Van Dijk N, Merlo L, Aricò AS. Enhanced performance and durability of low catalyst loading PEM water electrolyser based on a short-side chain perfluorosulfonic ionomer. Appl Energy 2017;192:477–89. https://doi.org/10.1016/j.apenergy.2016.09.011.

[45] Yu H, Danilovic N, Wang Y, Willis W, Poozhikunnath A, Bonville L, et al. Nano-size IrOx catalyst of high activity and stability in PEM water electrolyzer with ultra-low iridium loading. Appl Catal B Environ 2018;239:133–46. https://doi.org/10.1016/J.APCATB.2018.07.064.

[46] Stassi A, Gatto I, Baglio V, Passalacqua E, Aricò AS. Oxide-supported PtCo alloy catalyst for intermediate temperature polymer electrolyte fuel cells. Appl Catal B Environ 2013;142–143:15–24. https://doi.org/10.1016/j.apcatb.2013.05.008.

[47] Dinh Nguyen MT, Ranjbari A, Catala L, Brisset F, Millet P, Aukauloo A. Implementing molecular catalysts for hydrogen production in proton exchange membrane water electrolysers. Coord Chem Rev 2012;256:2435–44. https://doi.org/10.1016/j.ccr.2012.04.040.

[48] Siracusano S, Hodnik N, Jovanovic P, Ruiz-Zepeda F, Šala M, Baglio V, et al. New insights into the stability of a high performance nanostructured catalyst for sustainable water electrolysis. Nano Energy 2017;40:618–32. https://doi.org/10.1016/j.nanoen.2017.09.014.

[49] Saveleva VA, Wang L, Kasian O, Batuk M, Hadermann J, Gallet JJ, et al. Insight into the Mechanisms of High Activity and Stability of Iridium Supported on Antimony-Doped Tin Oxide Aerogel for Anodes of Proton Exchange Membrane Water Electrolyzers. ACS Catal. 2020;10:2508–16. https://doi.org/10.1021/ACSCATAL.9b04449.

[50] Rozain C, Mayousse E, Guillet N, Millet P. Influence of iridium oxide loadings on the performance of PEM water electrolysis cells: Part I–Pure IrO2-based anodes. Appl Catal B Environ 2016;182:153–60. https://doi.org/10.1016/J.APCATB.2015.09.013.

[51] Lee B-S, Ahn SH, Park H-Y, Choi I, Yoo SJ, Kim H-J, et al. Development of electrodeposited IrO2 electrodes as anodes in polymer electrolyte membrane water electrolysis. Appl Catal B Environ 2015;179:285–91. https://doi.org/10.1016/J.APCATB.2015.05.027.

[52] Cruz JC, Ramos Hernández A, Guerra-Balcazar M, Chávez-Ramirez AU, Ledesma-García J, Arriaga LG. Electrochemical evaluation of a Ir-Ru binary oxide for oxygen evolution reaction. Int J Electrochem Sci 2012;7:7866–76.

[53] Marshall A, Børresen B, Hagen G, Tsypkin M, Tunold R. Hydrogen production by advanced proton exchange membrane (PEM) water electrolysers-Reduced energy consumption by improved electrocatalysis. Energy 2007;32:431–6. https://doi.org/10.1016/J.ENERGY.2006.07.014.

[54] Siracusano S, Stassi A, Baglio V, Aricò AS, Capitanio F, Tavares AC. Investigation of carbon-supported Pt and PtCo catalysts for oxygen reduction in direct methanol fuel cells. Electrochim Acta 2009;54:4844–50. https://doi.org/10.1016/j.electacta.2009.03.070.

[55] Skulimowska A, Dupont M, Zaton M, Sunde S, Merlo L, Jones DJ, et al. Proton exchange membrane water electrolysis with short-side-chain Aquivion® membrane and IrO2 anode catalyst. Int J Hydrogen Energy 2014;39:6307–16. https://doi.org/10.1016/j.ijhydene.2014.02.082.

[56] Siracusano S, Baglio V, Moukheiber E, Merlo L, Aricò AS. Performance of a PEM water electrolyser combining an IrRu-oxide anode electrocatalyst and a short-side chain Aquivion membrane. Int J Hydrogen Energy 2015;40:14430–5. https://doi.org/10.1016/J.IJHYDENE.2015.04.159.

[57] Elsøe K, Grahl-Madsen L, Scherer GG, Hjelm J, Mogensen MB. Electrochemical Characterization of a PEMEC Using Impedance Spectroscopy. J Electrochem Soc 2017;164:F1419–26. https://doi.org/10.1149/2.0651713jes.

[58] Siracusano S, Van Dijk N, Payne-Johnson E, Baglio V, Aricò AS. Nanosized IrOx and IrRuOx electrocatalysts for the O2 evolution reaction in PEM water electrolysers. Appl Catal B Environ 2015;164:488–95. https://doi.org/10.1016/j.apcatb.2014.09.005.

[59] Siracusano S, Baglio V, Grigoriev SA, Merlo L, Fateev VN, Aricò AS. The influence of iridium chemical oxidation state on the performance and durability of oxygen evolution catalysts in PEM electrolysis. J Power Sources 2017;366:105–14. https://doi.org/10.1016/j.jpowsour.2017.09.020.

[60] Fouda-Onana F, Chandesris M, Médeau V, Chelghoum S, Thoby D, Guillet N. Investigation on the degradation of MEAs for PEM water electrolysers part I: Effects of

testing conditions on MEA performances and membrane properties. Int J Hydrogen Energy 2016;41:16627–36. https://doi.org/10.1016/J.IJHYDENE.2016.07.125.

[61] Frensch SH, Serre G, Fouda-Onana F, Jensen HC, Christensen ML, Araya SS, et al. Impact of iron and hydrogen peroxide on membrane degradation for polymer electrolyte membrane water electrolysis: Computational and experimental investigation on fluoride emission. J Power Sources 2019;420:54–62. https://doi.org/10.1016/J.JPOWSOUR.2019.02.076.

[62] Siracusano S, Trocino S, Briguglio N, Pantò F, Aricò AS. Analysis of performance degradation during steady-state and load-thermal cycles of proton exchange membrane water electrolysis cells J Power Sources, 2020; 468:228390. https://doi.org/10.1016/j.jpowsour.2020.228390.

[63] Tsotridis G, Pilenga A. EU harmonised terminology for low-temperature water electrolysis for energy-storage applications, JRC Technical Reports, EU Commission, ISBN: 978-92-79-90387-8 (online); 1831-9424 (online), https://doi.org/10.2760/138987 (online).

SUPPLEMENTARY DATA

Durability of a recombination catalyst-based membrane-electrode assembly for electrolysis operation at high current density

Fabiola Pantò, Stefania Siracusano, Nicola Briguglio, Antonino Salvatore Aricò*

CNR-ITAE Institute of Advanced Energy Technologies, National Research Council

Via Salita S. Lucia sopra Contesse 5, 98126 Messina, Italy

**Corresponding author: Tel.: +39 090 624237; fax: +39 090 624247. E-mail address: arico@itae.cnr.it*

Additional figures

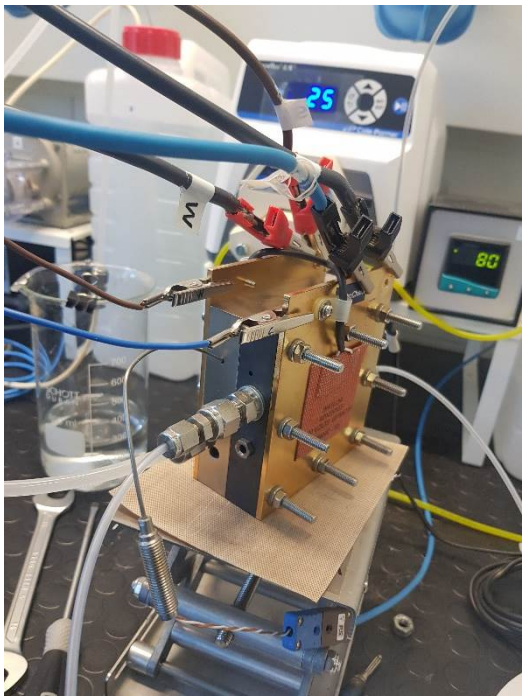

Fig. S1 Electrolysis cell housing equipped with titanium and graphite plates.

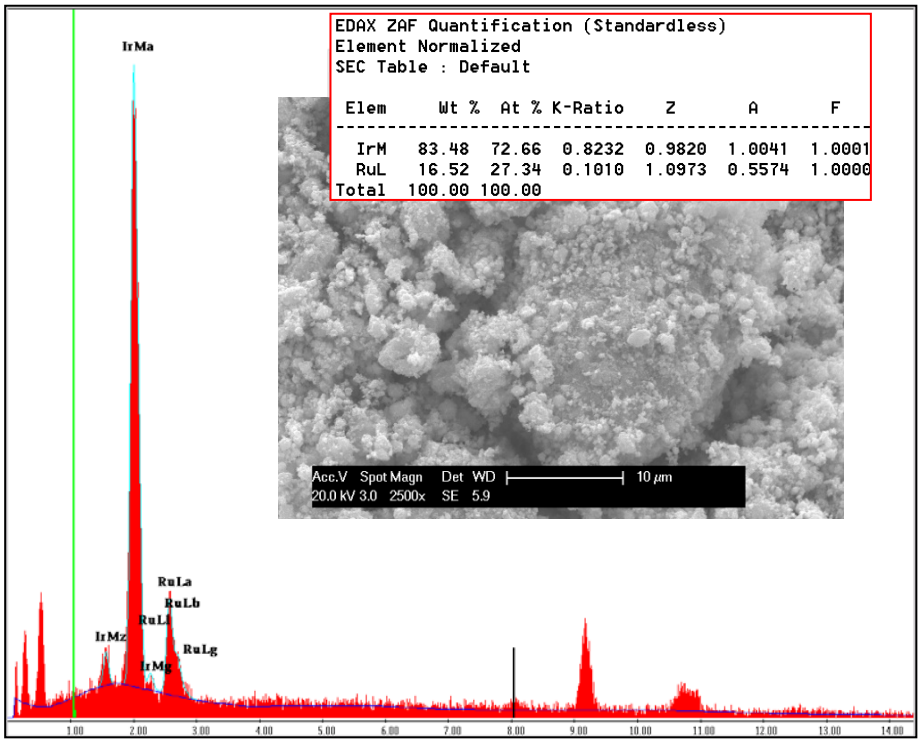

Fig. S2 SEM image and the EDX spectrum of IrRuOx (Ir:73% at. Ru: 27% at.) catalyst.

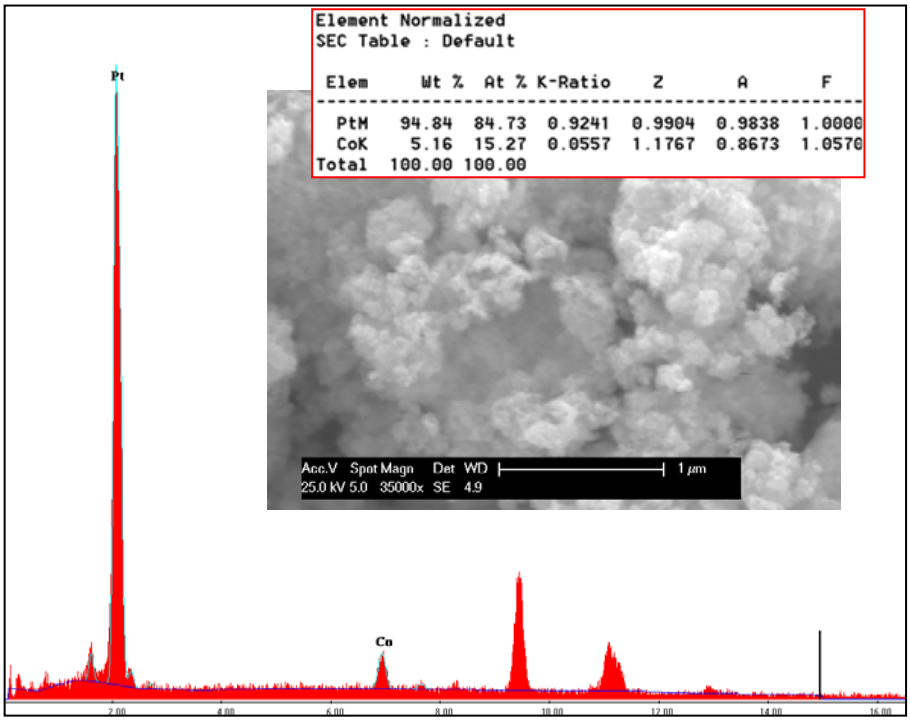

Fig. S3 SEM image and the EDX spectrum of PtCo (Pt:85% at. Co: 15% at.) catalyst.

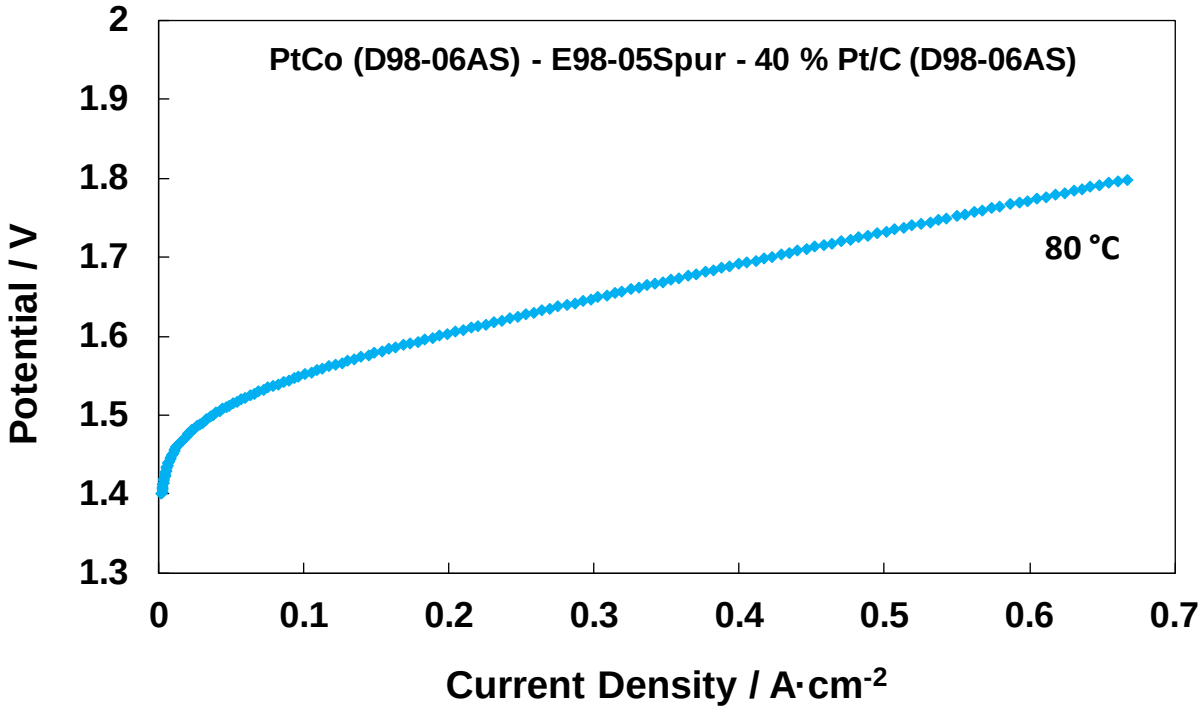

Fig. S4 Polarisation at 80 °C for the MEA containing the PtCo as anode catalyst.

Determination of cell voltage efficiency

Ideally, the PEM electrolysis cell can operate adiabatically with no exchange of thermal energy with the environment at the so-called thermoneutral potential, E_{tn}, which is defined, under standard (SATP) conditions, by:

$E_{tn} = \Delta H°/(n \cdot F)$ [Ref. S1]

where $\Delta H°$ is the standard reaction enthalpy, n is equal to 2 (number of electrons involved in the formation of one hydrogen molecule from a water molecule) and F is the Faraday constant i.e. 96485 C.
The total energy required by the electrolysis process $\Delta H°$ is the sum of the thermal energy requirements $\Delta Q_{rev} = T\Delta S°$ (where $\Delta S°$ is the entropy variation and T is the absolute temperature) and the electrical energy needs, $\Delta G°$, also known as the Gibbs free energy change of the reaction according to the Gibbs-Helmholtz equation:

$\Delta H° = \Delta G° + T\Delta S°$

Under SATP conditions corresponding to 298.15 K (25 °C) and 101 kPa (essentially 1 atmosphere, $\Delta H°$ = HHV = 285.8 kJ mol^{-1}. The higher heating value (HHV) includes the heat of water vaporisation and is used as a reference for liquid water electrolysis. The cell voltage corresponding to the HHV is thus E_{tn} = 1.48 V.

The overall efficiency under standard conditions is calculated according to the following equation:

$$\eta = \frac{energy\ content\ of\ reaction\ products}{total\ energy\ requirements} = \frac{\Delta H°}{Total\ energy\ input}$$

At 4 A cm^{-2} and 80°C the recorded cell voltages from the polarisation curves in Fig. 7 (main text) are 1.83 V and 1.85 V. These are well above the thermoneutral potential and the reaction is highly exothermic under such conditions. Thus, no heat transfer to the cell is needed.

At 80°C and 101 kPa, E_{tn} slightly decreases to E_{tn}= 1.47 V [Ref. S1].

Under such conditions, the voltage efficiency referred to the HHV can be calculated from the following equation:

$$\eta_v = \frac{E_{tn}}{E_{cell}}$$

Thus, after 3500 h operation, the cell voltage efficiencies at 4 A cm^{-2} derived from the polarisation curves in Fig. 7 (main text) are:

80% and 79% for the recombination catalyst-based MEA and the bare MEA.

References

[S1] G.Tsotridis, A. Pilenga EU harmonised terminology for low-temperature water electrolysis for energy-storage applications, JRC Technical Reports, EU Commission, ISBN: 978-92-79-90387-8 (online); 1831-9424 (online), DOI: 10.2760/138987 (online)]